Delivery report

PV-LAC: advances Land, Aerosol and Coastal products for Proba-V

PV-LAC: D-2-A3 ATBD Activity 3 & D-3-A3 IODD Activity 3

Sindy Sterckx, Nitin Bhatia

November 2016

DISTRIBUTION LIST

Author(s)	:	Sindy Sterckx, Nitin Bhatia
Reviewer(s)	:	Philippe Goryl, Fabrizio Niro
Approver(s)	:	Philippe Goryl, Fabrizio Niro
Issuing authority	:	VITO

CHANGE RECORD

Release	Date	Pages	Description of change	Editor(s	Reviewer(s)
V1.1	13/11/2016	All	First version	Sindy Sterckx, Nitin Bhatia	Philippe Goryl, Fabrizio Niro

TABLE OF CONTENTS

LIST OF FIGURES

LIST OF TABLES

ACONYMS

LUT	Look-Up Table
SMAC	Simplified Method for Atmospheric Correction
TOA	Top-of-Atmosphere
TOC	Top-of-Canopy
IODD	Input-output Definition Document
ATBD	Algorithm Theoretical Basis Document
TSM	Total Suspended Matter
NIR	Near-Infrared
SWIR	Shortwave Infrared
MODTRAN	MODerate resolution atmospheric TRANsmission
SZA	Solar zenith angle
VZA	Viewing zenith angle
RAA	Relative azimuth angle
AOT	Aerosol Optical Thickness
DISORT	DIScrete Ordinate Radiance Transfer
S1	1-daily synthesis
ECMWF	European Centre for Medium-Range Weather Forecast
OPERA	Operational atmospheric correction for Land and Water
VITO	Vlaamse Instelling voor Technologisch Onderzoek
CEOS	Committee on Earth Observation Satellites
ACIX	Atmospheric correction intercomparison exercise
NDVI	Normalized Difference Vegetation Index
AERONET-OC	Aerosol Robotic Network – Ocean
FTU	Formazin Turbidity Unit
NTU	Nephelometric Turbidity Unit
MODIS	Moderate Resolution Imaging Spectroradiometer
SM	Status map
ASCII	American Standard Code for Information Exchange

CHAPTER 1 INTRODUCTION

This is the first version (V1) of the ATBD and IODD.

The structure of the document is as follows :

In CHAPTER 2 provides the ATBD for the atmospheric correction. The algorithmic basis for two approaches for the retrieval of the aerosol information i.e. (1) spatial extension of the AOT values retrieved from nearby land and (2) Retrieval of aerosol information from the SWIR band following a SWIR black pixel approach over water.

In CHAPTER 3 the ATBD for three different algorithms for TSM or Turbidity retrieval from PROBA-V data is given. A preliminary testing of the algorithms is performed on the basis of several test datasets which contain in-situ measured water leaving reflectance spectra resampled to the PROBA-V spectral bands and corresponding TSM/Turbidity concentrations.

CHAPTER 4 provides the preliminary IODD for both the atmospheric correction and TSM/Turbidity prototype processors.

CHAPTER 2 ATMOSPHERIC CORRECTION

2.1. TOA SIGNAL DECOMPOSITION

Following Ruddick et al. (2008) the radiance received by the PROBA-V instrument at the top-of-atmosphere level (TOA), L_{tot}^{TOA}, can be decomposed as (radiance terms for contribution from adjacent terrestrial areas are omitted here for the sake of simplicity)

$$L_{tot}^{TOA} = L_{path}^{TOA} + L_{int}^{TOA} + L_{w}^{TOA} \quad (2.1)$$

where

L_{path}^{TOA} the atmospheric path radiance (photons which have undergone at least one scattering in the air and none in the water)

L_{int}^{TOA} the photons that have scattered exactly once at the air-sea interface and none in the air or water and reach the TOA

L_{w}^{TOA} the photons that have scattered at least once in the water and reach the TOA

The atmospheric path radiance term (L_{path}^{TOA}) can be further decomposed as

$$L_{path}^{TOA} = L_{a}^{TOA} + L_{r}^{TOA} + L_{ar}^{TOA} \quad (2.2)$$

where

L_{a}^{TOA} the TOA radiance due to scattering by aerosols only

L_{r}^{TOA} the TOA radiance due to scattering by air molecules only (Rayleigh scattering)

L_{ar}^{TOA} the TOA radiance due to aerosol-molecule scattering

L_{int}^{TOA} can be partitioned into

$$L_{int}^{TOA} = L_{g}^{TOA} + L_{wc}^{TOA} \quad (2.3)$$

where

L_{g}^{TOA} the direct sun glint radiance that reaches the TOA

L_{wc}^{TOA} the radiance reflected by white caps and foam that reaches the TOA

The other air/sea reflections, such as the skylight reflectance, are in most papers defined within L_{path}^{TOA} or L_{w}^{TOA}. Here it will be accounted for in the L_{w}^{TOA} term (see eq. 2.12 and 2.13).

If we ignore the surface foam and white caps reflectance, and the specular reflection of direct sun (see for further discussions in section 2.7 and 2.8) , equation (1) can be simplified to

$$L_{tot}^{TOA} = L_{a}^{TOA} + L_{r}^{TOA} + L_{ar}^{TOA} + L_{w}^{TOA} \quad (2.4)$$

If we express the TOA signal in terms of TOA reflectance ρ_{tot}^{TOA} with

$$\rho_{tot}^{TOA} = \pi L_{tot}^{TOA} / (E_0 \cos(\theta_s) \left[\frac{d_0}{d}\right]^2) \quad (2.5)$$

where

E_0 the extra-terrestrial solar irradiance integrated over the spectral response of the different PROBA-V spectral bands

θ_s the solar zenith angle,

$\frac{d_0}{d}$ the ratio of Sun-Earth distance at the acquisition date to the mean Sun-Earth distance.

and decouple the gaseous absorption (by Ozone and water vapor) and scattering, equation (4) becomes

$$\rho_{tot}^{TOA} = T_g \left(\rho_a^{TOA,c} + \rho_r^{TOA,c} + \rho_{ar}^{TOA,c} + \rho_w^{TOA,c}\right) \quad (2.6)$$

where

T_g the two-way transmittance (sun-to-surface and surface-to-sensor) due to Ozone (O_3) and water vapor (H_2O) gaseous absorption.

Formulating ρ_w^{TOA} at the surface level and considering multiple reflections between the water body and the atmosphere equation (6) becomes (Frouin and Pelletier, 2015)

$$\rho_{tot}^{TOA} = T_g \left(\rho_a^{TOA,c} + \rho_r^{TOA,c} + \rho_{ar}^{TOA,c} + T \frac{R_w}{(1-sR_w)}\right) \quad (2.7)$$

and equation (4) becomes

$$L_{tot}^{TOA} = T_g \left(L_{path}^{TOA,c} + T \frac{R_w E_0 \cos(\theta_s) \left[\frac{d_0}{d}\right]^2}{\pi(1-sR_w)}\right) \quad (2.8)$$

where

s is the spherical albedo of the atmosphere (Chandrasekhar, 1960). Multiple reflections between the water body and the atmosphere are approximated by multiplying R_w by $(1-sR_w)^{-1}$

T is the two-way (sun-to-surface and surface-to-sensor) total (direct and diffuse) atmospheric transmittance.

For simplicity we introduce the 'G-factor' with $G = T \frac{E_0 \cos(\theta_s) \left[\frac{d_0}{d}\right]^2}{\pi}$. Equation (8) becomes

$$L_{tot}^{TOA} = T_g \left(L_{path}^{TOA,c} + G \frac{R_w}{(1-sR_w)}\right) \quad (2.9)$$

Solving equation (9) for R_w gives :

$$\rho_w = \frac{L_{tot}^{TOA,c} - L_{path}^{TOA,c}}{G + s(L_{tot}^{TOA,c} - L_{path}^{TOA,c})} \quad (2.10)$$

with

$$L_{tot}^{TOA,c} = \frac{L_{tot}^{TOA}}{T_g} \quad (2.11)$$

In the used formulation R_w still contains the skylight reflectance (i.e. the reflection of diffuse light by the air-water interface). R_w is corrected for the remaining air-sea interface effects using the following equation (Brando and Dekker, 2003; De Haan et al., 1996):

$$\rho_w = R_w - d \quad (2.12)$$

with

$$d = \pi . r . L_d / E_d \quad (2.13)$$

where

r the Fresnel reflectance. It can be calculated taking into account the refraction indices of sea water and air and the angles of incidence and refraction

L_d the sky radiance

E_d the downwelling irradiance just above the sea surface

The goal of atmospheric correction is to retrieve the water leaving reflectance (ρ_w) from the TOA signal after factoring out the other components (T_g, the G-factor (G), the path radiance ($L_{path}^{TOA,c}$) , spherical albedo (S) and the sky-glint correction term (d)). This is done by modeling the scattering and absorption properties of the atmosphere with radiative transfer codes (see 2.3) based on solar and viewing angles, atmospheric pressure, the aerosol optical thickness and the aerosol model.

2.2. GASEOUS TRANSMITTANCE

The PROBA-V TOA radiance is impacted by absorption by Ozone (O_3), water vapor (H_2O) and Oxygen (O_2) as illustrated in Figure 1.

To take into account spatial and temporal variation of O_3, and H_2O either the atmospheric LUT (see section 2.3) can be calculated for a range of O_3 and H_2O concentrations or correction for gaseous absorption can be done before the atmospheric correction assuming decoupling of scattering and absorption processes. Here, we use this latter option as given by equation (2.11) in order to reduce the size of the LUT. Please note that correction that T_g will here not include oxygen. Absorption by oxygen will be included the LUT correction parameters.

The gaseous transmittance is calculated based on actual concentration and the airmass (M) using the SMAC coefficients calculated for PROBA-V and used in the nominal processing of PROBA-V.

The gaseous transmittance can be calculated as follows :

$$T_g^k(U_{gas}, M) = exp\left(a_{gas}^k . (M . U_{gas})\text{^}n_{gas}^k\right) \quad (2.14)$$

Where

$U_{gas}$is the actual gaseous concentration of ozone or water vapor (total amount ozone in units of cm/atm and water vapor in kg/cm²)

k denotes the spectral band

M is the airmass

a_{gas}^k , n_{gas}^k the pre-calculated SMAC coefficients for ozone or water vapor. The actual values are given in Table 1.

The airmass M is calculated based on the solar and view zenith angle as

$$M = \frac{1}{(\cos(\theta_s) + \cos(\theta_v))} \tag{2.15}$$

With

θ_s the solar zenith angle

θ_v the view zenith angle

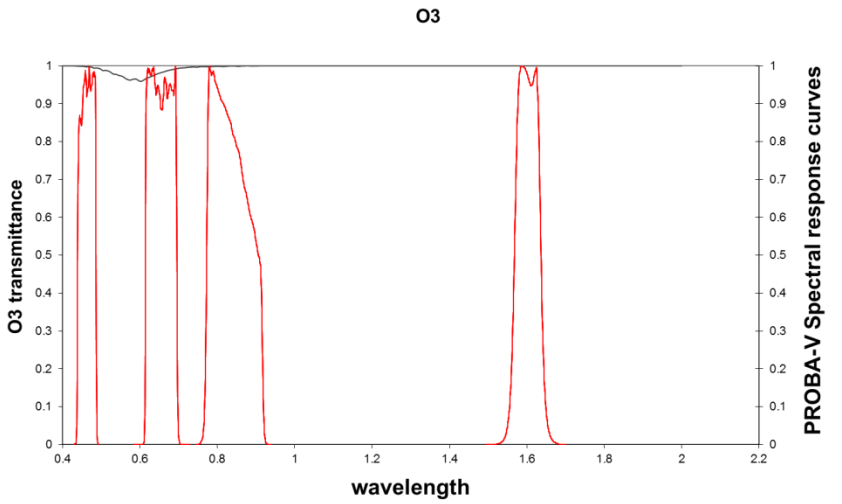

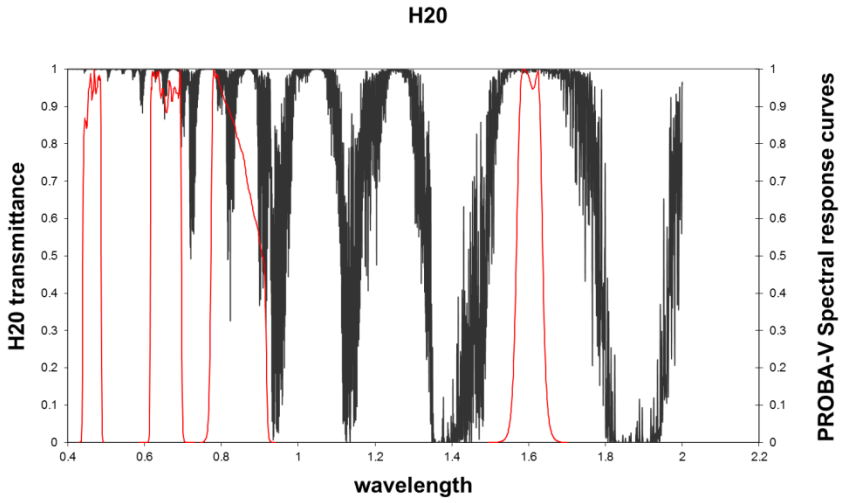

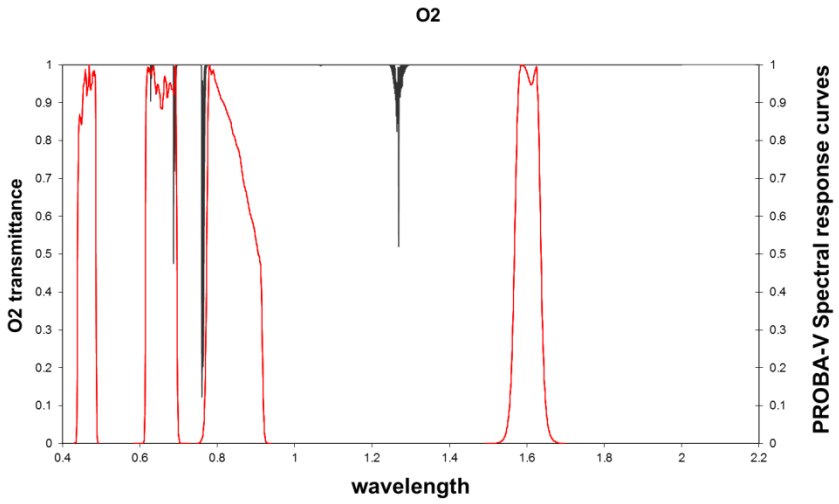

Figure 1. Gaseous absorption in PROBA-V bands (Red lines: spectral response curves center Camera, Black lines: gaseous transmittance).

Table 1. SMAC coefficients for ozone or water vapor for the PROBA-V bands

	BLUE		RED		NIR		SWIR	
	a	*n*	*a*	*n*	*a*	*n*	*a*	*n*
O3	-0.00816	0.998394	-0.06409	0.994402	-3E-05	0.950666		
H2O			-0.00365	0.745874	-0.03822	0.524552	-0.00065	0.942148

2.3. MODTRAN LUT GENERATION

The Moderate-Resolution Atmospheric Radiance and Transmittance Model-5 "MODTRAN5" (Berk *et al.,* 2006) is used for the radiative transfer calculation. This section describes the generation of the look-up tables required for both the aerosol retrieval and the actual atmospheric correction step.

MODTRAN based radiative transfer modelling has been used in various (turbid) water atmospheric correction schemes (Sterckx et al., 2011; Arabi et al., 2016; Brando and Dekker, 2003).

As MODTRAN5 cannot directly be inverted to retrieve the surface reflectance, the MODTRAN interrogation technique is used for atmospheric correction purposes (Verhoef *et al.* 2003; De Haan et al., 1996). The technique consists of running MODTRAN5 for three different surface albedos (i.e. 0.0, 0.5 and 1.0). This allows to derive the three atmospheric correction parameters required within equation (8) i.e. (the G-factor (G), path radiance ($L_{path}^{TOA,c}$), and spherical albedo (s). For the calculation the sky glint correction term (d) two extra MODTRAN5 runs are required. These parameters are convolved with the spectral response functions of the PROBA-V bands to compute the correction parameters for every band.

The different parameters (G-factor (G), path radiance ($L_{path}^{TOA,c}$), spherical albedo (s) and *d*-coefficient) are pre-calculated with MODTRAN 5 in function of view zenith angle, solar zenith angle, relative azimuth angle, AOT and aerosol model and stored in LUT. The LUT specifications are given in Table 5. The optimum breakpoints positions for the different input parameters will be determined taking into account a tradeoff between sufficient sampling and LUT size.

Table 2. Parameter setting MODTRAN5 LUT simulations

Parameter	Range or Value
Atmospheric profile	Mid-latitude summer
CO2	360 ppm
H2O*	0
O3*	0
AOT	0-0.7
SZA	0-70°
VZA	0-20°
RAA	0°-155°
Aerosol Model	Rural (ihaze1), Maritime (ihaze 4), Urban (ihaze 5)
Surface height	0
Scattering method	DISORT 16-stream multiple scattering
Solar irradiance	Thuillier et al. (2003)

**H2O and O3 concentration are set to zero as the PROBA-V data will be corrected first for gaseous absorption*

The lowest AOT value is set to zero. It allows to use the LUT to perform a correction for the Rayleigh scattering only as for instance used in the SWIR based aerosol retrieval step (see section 2.9.2). The DISORT (DIScrete Ordinate Radiance Transfer) is selected to properly account for the azimuthal dependency of multiple scattering as indicated by Campbell et al. (2011). Berk et al. (2005) showed that the spectral radiance predictions in the visible spectral region (400-700nm) with ISAACS multiple scattering can be 10% below the results obtained with DISORT depending on the atmospheric and observation conditions. The Thuillier *et al.* (2003) sun irradiance spectrum is preferred instead of the standard extraterrestrial solar irradiance models included in MODTRAN. Please note that the Thuillier *et al.* 2003) sun irradiance spectrum is also used in the vicarious calibration performed within the Image Quality Center and for the nominal processing of the PROBA-V data to calculate the TOA reflectance. The LUTs will be generated for three standard MODTRAN aerosol types (i.e. rural, urban and maritime aerosols).

In Figure 2 some examples are given of the path radiance ($L_{path}^{TOA,c}$), gain factor (G), spherical albedo (s) and sky glint correction (d-term) calculated with MODTRAN for various atmospheric conditions (i.e. aerosol types and AOT values). As Figure 2 shows the path radiance, spherical albedo and sky-glint (d-term) decreases with wavelength and increases with AOT. The urban aerosol has a stronger absorption and therefore showing lower values compared to the maritime and rural aerosols.

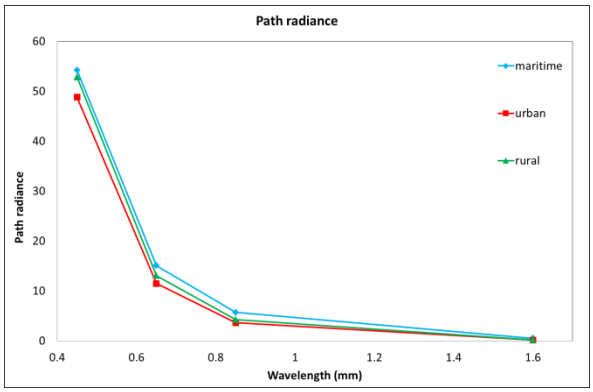

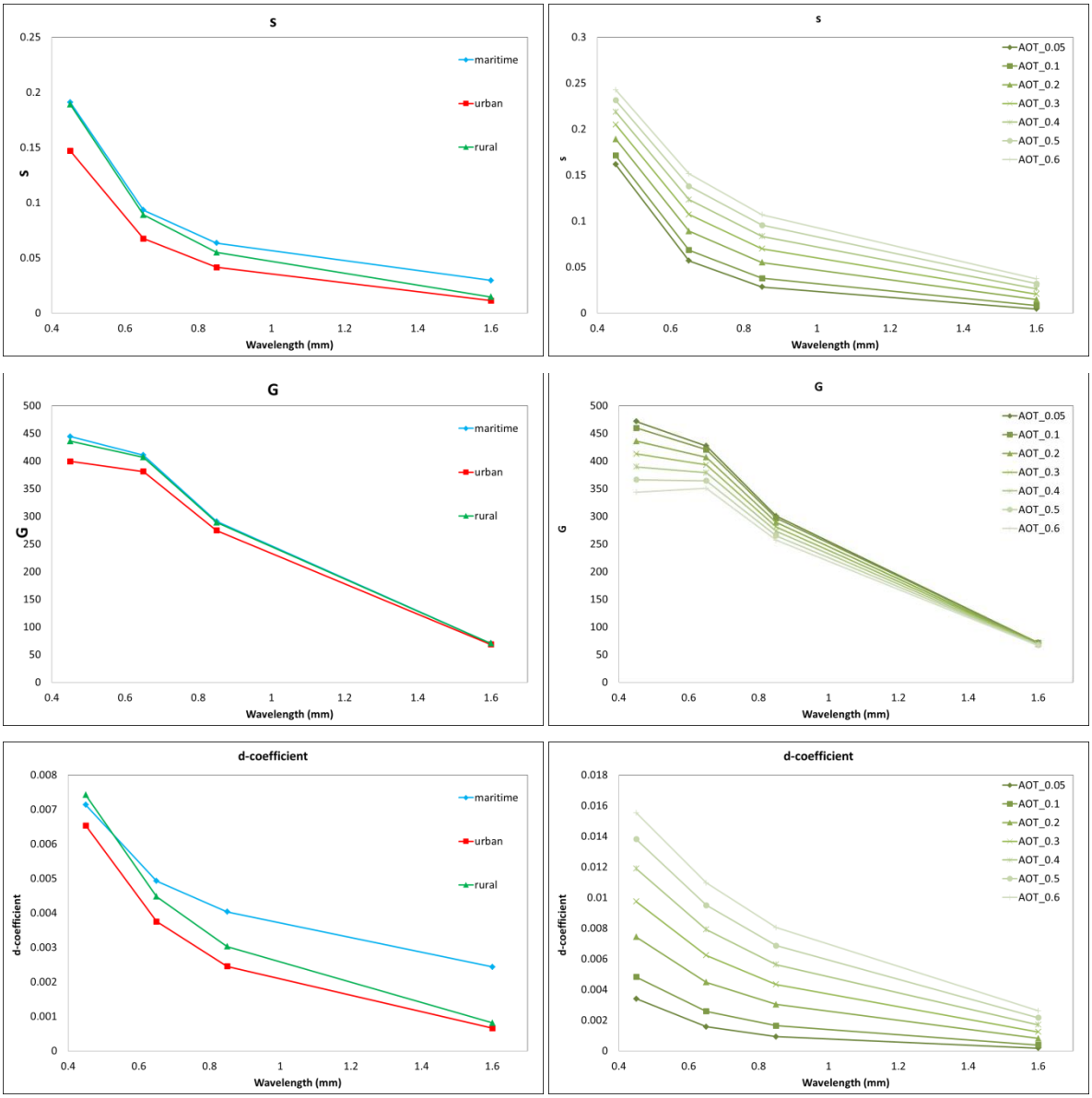

Figure 2. $L_{path}^{TOA,c}$, G, S and d values for PROBA-V bands calculated with MODTRAN5 for a nadir observation and SZA of 20°. Left: parameters are given for maritime, rural and urban aerosol for an AOT value of 0.2; Right: parameters are given for rural aerosol only but for varying AOT values (between 0.05 and 0.6).

2.4. OVERALL WORKFLOW

In Figure 3 the flowchart for the atmospheric correction is given.

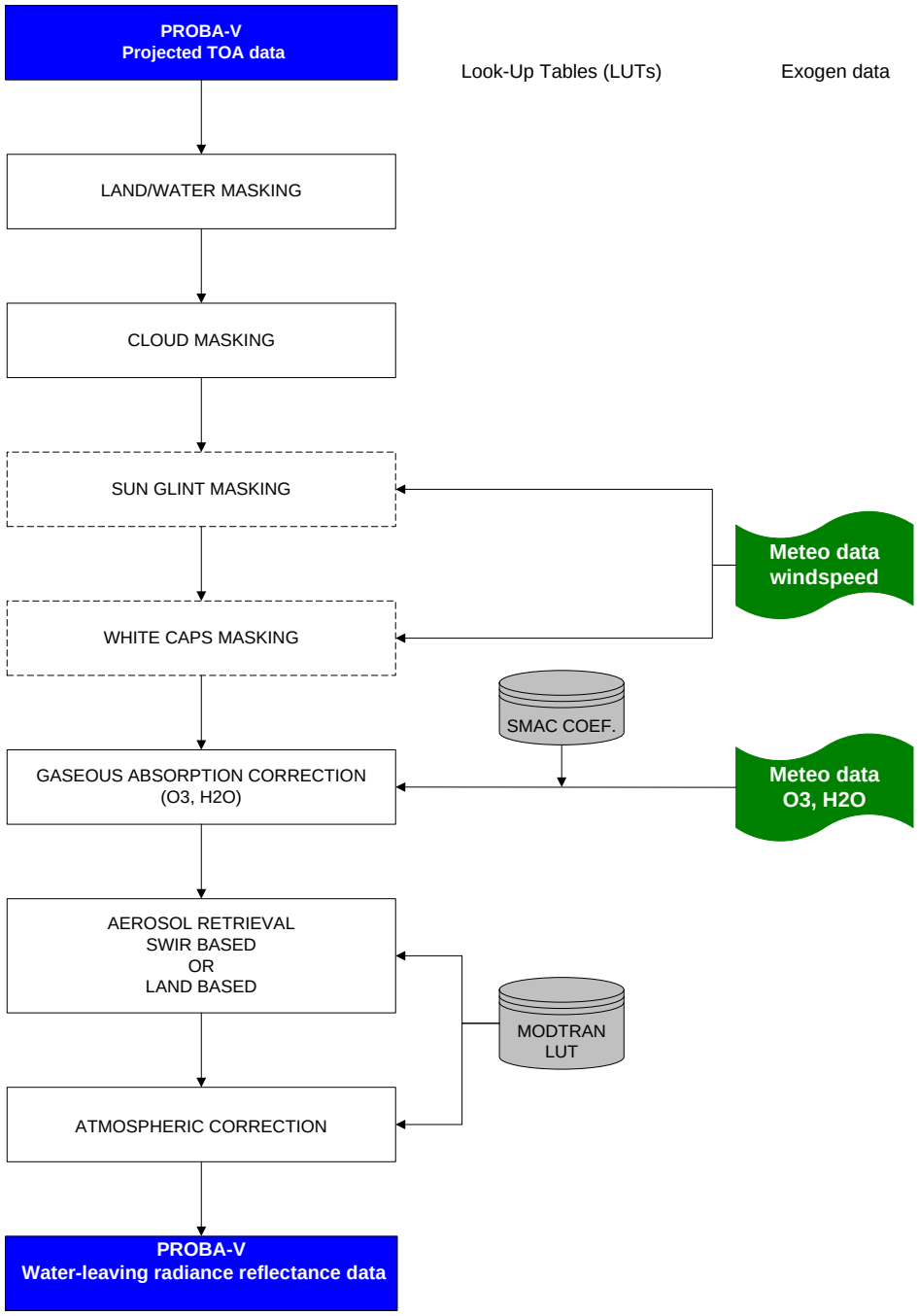

Figure 3. Overall atmospheric correction workflow

The atmospheric correction starts from projected TOA data. These can be either S1 100 m products or the L2A products which will be made available in the reprocessed collection.

First, a simple land/water and cloud masking is performed as further detailed in section 2.5 and 2.6, respectively.

On the basis of wind speed meteo data water areas affected by sun glint or white caps can be masked as detailed in section 2.5 and 2.8, respectively. It should be noted that the current meteo data used in the PROBA-V processing facility do not contain wind speed information. Wind speed data can be freely downloaded from ECMWF ERA Interim

(http://apps.ecmwf.int/datasets/data/interim-full-daily/) at a spatial resolution of 0.75 degrees. The data are made available with an offset of about three months.

Next a cloud mask is generated where in addition to the nominal PROBA-V cloud mask an extra check on the SWIR band is added over water (see section 2.6).

In order to reduce the atmospheric correction LUT size and complexity of the LUT interpolation a correction performed for the ozone and water vapor gaseous absorption using the available SMAC coefficients (2.2).

Next the aerosol information is retrieved from the image. Two different approaches will be evaluated : 1) an approach based on spatial extension of aerosol information retrieved from nearby land (2.9.1) and a "black pixel" approach using the PROBA-V SWIR band (2.9.2).

Once the AOT (and aerosol type) is known the actual atmospheric correction parameter are calculated by a multi-parameter LUT interpolation.

2.5. LAND/WATER MASKING

A basic land/water is needed as input for the aerosol retrieval step where a distinction between land and water pixels is required.

The land/water masking is based on a simple threshold applied to the TOA reflectance in the PROBA-V SWIR band.

2.6. CLOUD MASKING

Cloud reflectance is high in the SWIR, whereas water presents a very low reflectance. In order to avoid under-detection of clouds through application of the nominal cloud mask an extra masking will be performed based on a threshold on the TOA reflectance in the SWIR band.

2.7. SUN GLINT MASKING

The size of sun glint spot is variable as it depends on the ocean surface roughness which is controlled by wind speed. The range of angles from which the sun glint can be observed is larger for an agitated sea.

The generated LUTs include a correction for sky glint, but not for direct sun glint. Pixels affected by sun glint should therefore be discarded. For a flat sea surface (zero wind speed) the specular reflectance or directly reflected light can be computed 'exactly' using the Snell-Fresnel laws. For a rough sea surface, the reflection is conditioned by the wind and therefore the sun glint reflectance of the sea surface can only be described on statistical basis in function of wind speed. Cox-Munk (Cox and Munk, 1954) formalism is commonly used to calculate the wind speed-wave slope distribution. Here, we will adapt the isotropic Gaussian slope distribution (isotropic rough surface, independent of wind-direction) to represent the oceanic wave slopes. These isotropic wave slope PDF is often used in remote sensing applications when wind direction is not accurately known or not uniform.

Adopting this isotropic form, the probability of a spatial sample being contaminated by sun glint is given by :

$$P_{sg} = \frac{1}{\pi\sigma^2}\exp\left(-\frac{2(1+\cos(\theta_v)\cos(\theta_s)+\sin(\theta_v)\sin(\theta_s)\cos(\Delta\phi)) - (\cos(\theta_v)+\cos(\theta_s))^2}{\sigma^2(\cos(\theta_v)+\cos(\theta_s))^2}\right) \quad (2.16)$$

where

θ_s is the sun zenith angle (SZA) at the viewed spatial sample

θ_v is the view zenith angle (VZA) at the viewed spatial sample

$\Delta\phi$ is the relative azimuth angle (RAA)

σ^2 is the mean surface slope which is function of the windspeed ws as

$$\sigma^2 = 0.003 + 0.00512ws$$

The sun glint (specular) reflectance is given by:

$$\rho_{spe} = \frac{\pi r}{4\cos(\theta_s)\cos(\theta_v)\cos^4(\beta)} P_{sg} \quad (2.17)$$

where

r is the Fresnel reflection coefficient

β is the angle formed by the reflecting facet normal and the local normal defined by

$$\cos(\beta) = \frac{\cos(\theta_v)+\cos(\theta_s)}{\sqrt{2+2\cos(2\omega)}} \quad (2.18)$$

where

ω is the specular reflection angle defined by

$$\cos(2\omega) = \cos(\theta_v)\cos(\theta_s)+\sin(\theta_v)\sin(\theta_s)\cos(\Delta\phi)$$

The sun glint reflectance (ρ_{spe}) is independent of wavelength. Pixels with a ρ_{spe} value larger than a threshold. This threshold value is currently set to 0.005.

2.8. WHITECAPS MASKING

The sea surface might be largely contaminated by whitecaps especially for high wind speeds. In case wind speed information is available pixels or images contaminated by surface white caps can be discarded based on a wind speed threshold (10 m/s). For wind speeds lower than 10 m/s the whitecaps reflectance is small and can therefore be neglected.

2.9. AEROSOL RETRIEVAL

The main challenging components of the atmospheric are the retrieval of the AOT and aerosol type at the time of imaging. In D-1-A3 (Requirement Baseline Document) a review of different existing approaches was performed. Taking into account the specifications of PROBA-V, we will consider two methods: 1) based on spatial extension of aerosol information retrieved from nearby land and 2) based on extending the "black pixel" approach to the SWIR. The algorithmic implementation details of the methods are given in respectively section 2.9.1 and 2.9.2. Both approaches will be prototyped and their performance will be evaluated. Based on this performance assessment the most appropriate A/C approach will be selected and the next version of the ATBD will be updated accordingly. It is important to note that this final A/C approach might be a "merging" of both methods e.g. where for nearshore pixels a land-based approach is used, while for offshore pixels the NIR-SWIR approach is preferred.

2.9.1. LAND BASED AOT RETRIEVAL

The land based AOT retrieval approach originally described in Guanter *et al.* (2005) will be applied. In Guanter *et al.* (2010) the approach was used for the correction of inland water pixels where the AOT was retrieved through spatial extension of AOT values derived over neighboring land pixels following. The same approach is implemented in VITO's OPERA atmospheric correction code and is currently being evaluated on a large range of Landsat-8 and Sentinel-2 land and coastal scenes in the frame of the CEOS ACIX inter-comparison exercise (https://earth.esa.int/web/sppa/meetings-workshops/acix).

Aerosols are described by the aerosol model type (e.g. urban, desert, maritime aerosol) and the aerosol total loading giving by the aerosol optical depth (AOT) at 550nm. The aerosol model has to be selected a-priori as it has been reported in the past that it is very difficult to estimate the aerosol model (Ramon and Santer, 2005) over land. As PROBA-V has only 4 spectral bands this will be even more difficult.

The AOT retrieval algorithm makes use of the spectral variability of the land pixels within the image. The TOA image is subdivided into tiles which are small enough to assume atmospheric homogeneity and large enough to include high spectral variation. As a trade-off a tile size of 30x30 km is chosen. AOT retrieval is performed in a tile containing at least 35% cloud free pixels. To ensure that selected pixels are not affected by undetected clouds or cloud shadows the existing cloud mask is spatially extended. First, the lowest radiance value within the tile is selected for each VNIR band and the corresponding path radiance of this approximated dark target spectrum is retrieved using the pre-calculated MODTRAN5 LUT. The AOT value leading to the path radiance closest to the dark spectrum becomes the upper AOT boundary for the tile, not allowing path radiance to be higher than the dark spectrum in any of the spectral bands. In the next step, this initial AOT estimation will be refined. Five pixels with high spectral contrast are selected by means of multi-parameter inversion of TOA spectral radiances. These reference pixels are represented by the linear combination of a pre-defined vegetation and a soil spectrum to estimate the surface reflectance.

$$\rho_s = C_v * \rho_{veg} + C_s * \rho_{soil} \tag{2.19}$$

For every selected pixel, a set of $C_{v,s}$ parameters is used, which are free parameters in the inversion. This results in an 11-D inversion, with 2 parameters for every 5 pixels and AOT as degrees of freedom. In case the surface reflectance is higher than the end member, values larger than 1.0 are allowed for the parameters. The a priori selected spectra can be combined to reproduce the

actual shape of the reference pixels. By consequence, the selected pixels can act as end members; there is no need for image based end member retrieval.

The purpose of the contrast lies in the idea that for all cases the atmosphere above is invariant. The discriminant between contribution of the atmosphere and surface in the radiation of the TOA signal is used to characterize the AOT.

Practically, selection is based upon the pixel NDVI values from TOA reflectance, to eliminate the effect of different illuminations. The NDVI values are categorized in three classes: low [0.1-0.15], medium [0.15-0.45] and high [0.45-0.9], which are in pure soil, mixed and pure vegetation contributions. The number of selected pixels is not limited, but for computational time reasons set to 5. The inversion is then performed through the minimization of the following merit function:

$$\delta^2 = \sum_1^N \omega_{pix} \sum_{\lambda_i} \frac{1}{\lambda_i^2} \left[{L^{TOA,SIM}}_{pix,\lambda_i} - {L^{TOA,SENS}}_{pix,\lambda_i} \right]^2 \quad (2.20)$$

L^{SIM} is simulated TOA radiance, retrieved from the MODTRAN5 look-up table following equation 2.9, L^{SENS} is the measured TOA radiance. λ_i is the center wavelength for the *i* th band. To drive the inversion towards the lower wavelengths, the function is weighted by λ_i^{-2}.

ω_{pix} is the weighting factor, which is 2.0 for pure vegetation pixels, 1.5 for mixed and 1.0 for pure soil pixels to enhance the sensitivity in vegetation targets to aerosol loading.

The minimization of the merit function is done by the Powell's Minimization Method (Press et al., 1986. Initialization of the minimization algorithm is done through the result of the first step.

In order to minimize possible biases due to a bad representation of the actual surface reflectance by endmember combinations, three different vegetation spectra (Figure 4) are combined independently with one bare soil spectrum to simulate each reference pixel. The aerosol loading is calculated independently for each of the three pairs of vegetation and soil endmembers. The AOT value leading to the minimum value of the merit function driving the inversion is selected.

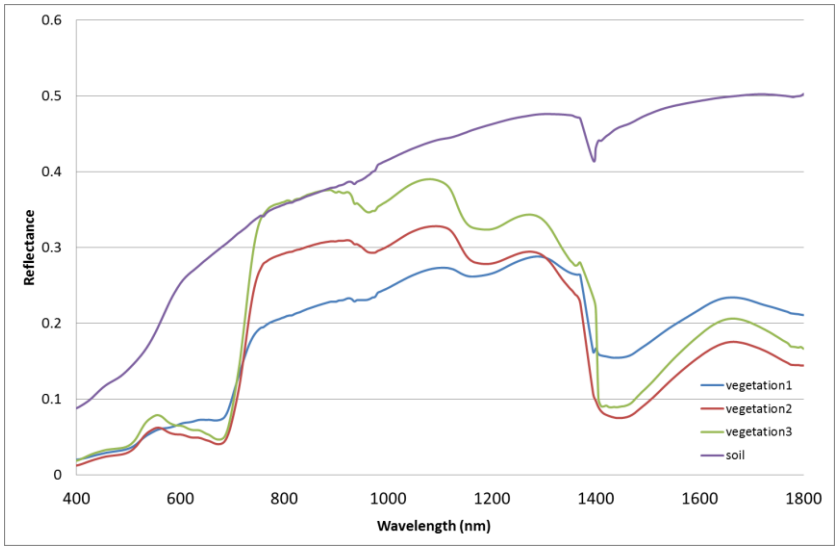

Figure 4. Spectral reflectance spectra of the four end members used in AOT retrieval

The last step in the AOT retrieval scheme is the interpolation of missing pixels and the smoothing of the resulting mosaic. The missing cells, deselected due to cloudiness or due to the land/sea mask, are interpolated from neighboring cells. To scale from cell image to per-pixel image, cubic convolution interpolation method is used.

The overall workflow is depicted in Figure 5.

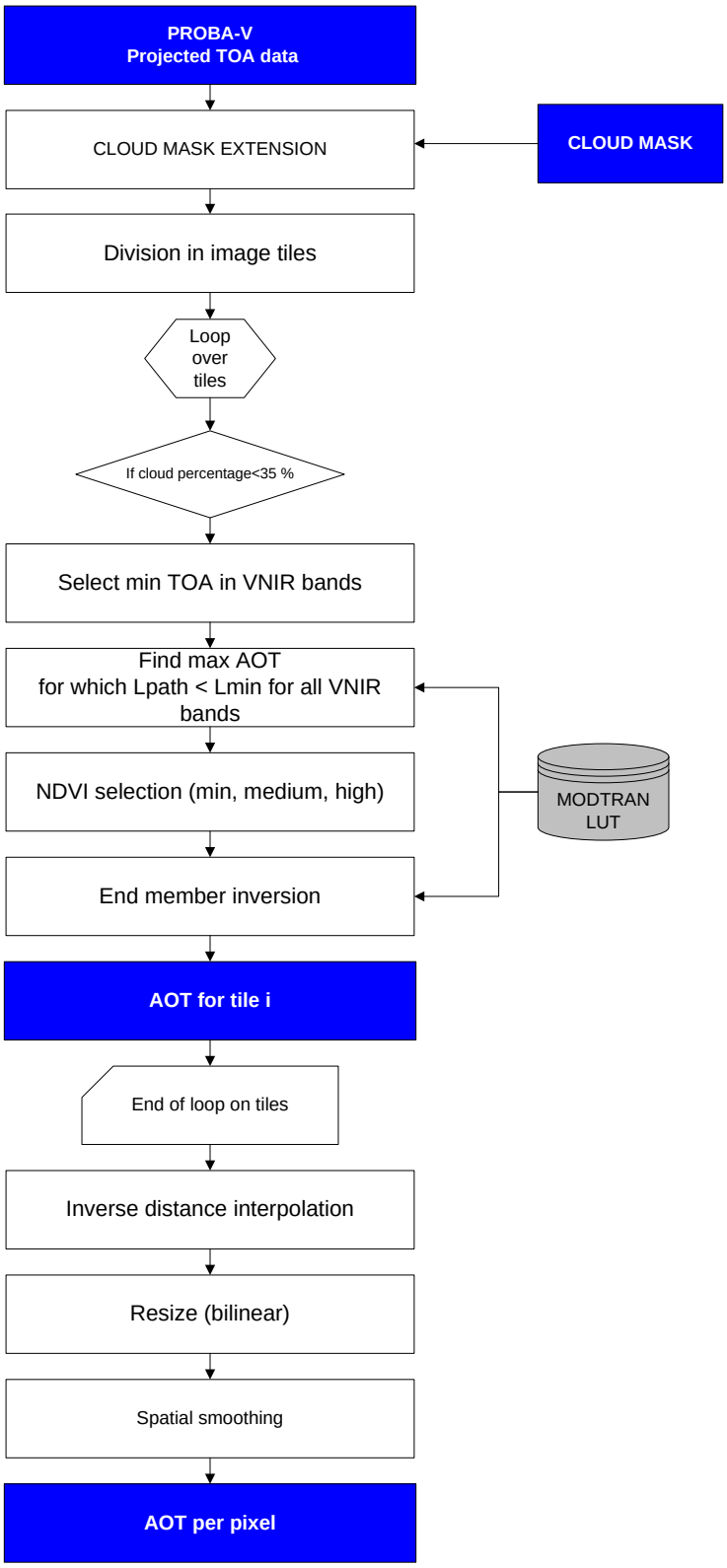

Figure 5. Flowchart land-based AOT retrieval

2.9.2. SWIR BLACK PIXEL METHOD

The SWIR black pixel approach assumes that the contribution of in-water constituents is zero due to the high absorption of pure water in the SWIR. The signal in the SWIR can thus be assumed to be entirely atmospheric and can therefore be employed for the aerosol determination.

In case there would be two SWIR bands available, the ratio of the TOA reflectance is used first for the aerosol type selection and in the next step the AOT is retrieved from one SWIR band.

For deriving the aerosol type, however, a fully SWIR based approach cannot be applied as PROBA-V has only 1 SWIR band.

Therefore either the aerosol model has to be fixed a priori as in the land-based approach or a alternative NIR-SWIR approach, like proposed by Vanhellemont and Ruddick (2015) for Landsat-8, has to be used. It requires the presence of clear water pixels which have to be selected first. For these clear water pixels the ratio of the aerosol reflectance at the NIR and SWIR is assumed to be constant and used to derive a scene constant aerosol type.

→ Clear pixel selection

To select the clear water pixels a correction for only Rayleigh contribution is performed using the MODTRAN5 LUT (section 2.3). We will denote the Rayleigh corrected reflectance as ρ_{cor}^{rayl}. Following Vanhellemont and Ruddick (2015) clear water pixels are selected based on the following criteria :

$$\frac{\rho_{cor}^{rayl}(NIR)+0.005}{\rho_{cor}^{rayl}(SWIR)} > 0.8 \text{ (TBC)} \quad (2.21)$$

The offset of 0.005 was included by Vanhellemont and Ruddick (2015) to retain low reflectance pixels where the band ratio is too restrictive (due to noise level). The offset of 0.005 and threshold of 0.8 will have to be re-evaluated for PROBA-V.

→ Aerosol selection

For the clear water pixels in the scene the ratio ($\epsilon^{NIR,SWIR}$) of the Rayleigh corrected reflectance is calculated :

$$\epsilon^{NIR,SWIR} = \rho_{cor}^{rayl}(NIR)/\rho_{cor}^{rayl}(SWIR) \quad (2.22)$$

The median value of $\epsilon^{NIR,SWIR}$ over the clear water pixels is then used to deduce the aerosol type. The retrieved $\epsilon^{NIR,SWIR}$ values are compared against pre-computed values tabulated for a suite of aerosol models (rural, urban, maritime) to select the appropriate aerosol model. In Table 3 the $\epsilon^{NIR,SWIR}$ for rural, urban and maritime aerosol as calculated with MODTRAN-5 for a SZA of 20°and an VZA of 0° is given. $\epsilon^{NIR,SWIR}$ can be derived pixel-by-pixel or as a single value per image using the median. The latter approach is selected as a pixel-by-pixel retrieval might introduce additional noise in the estimates of aerosol optical properties due to the typically low SNR in the SWIR bands.

	Urban	Rural	Maritime
$\epsilon^{NIR,SWIR}$	2.97 (+/- 0.21)	3.37 (+/- 0.028)	1.98 (+/- 0.33)

Table 3. $\epsilon^{NIR,SWIR}$ value as calculated with MODTRAN-5 for rural, urban and maritime aerosols for a SZA of 20°and an VZA of 0°

→ **AOT determination**

Once the aerosol model is determined, the AOT can be derived. The AOT per pixel is retrieved from the SWIR band based on the aerosol specific LUT which contains the atmospheric correction parameters in function of geometrical parameters and AOT. The AOT value for which the water leaving reflectance in the SWIR equals zero is searched for. In order to reduce the impact of the inherent noise in SWIR band on the retrieved AOT values. A spatial smoothing will be applied to PROBA-V SWIR data through application of a simple box-averaging approach as suggested by Wang and Shi (2012).

In Figure 6 a flowchart with the different steps is given.

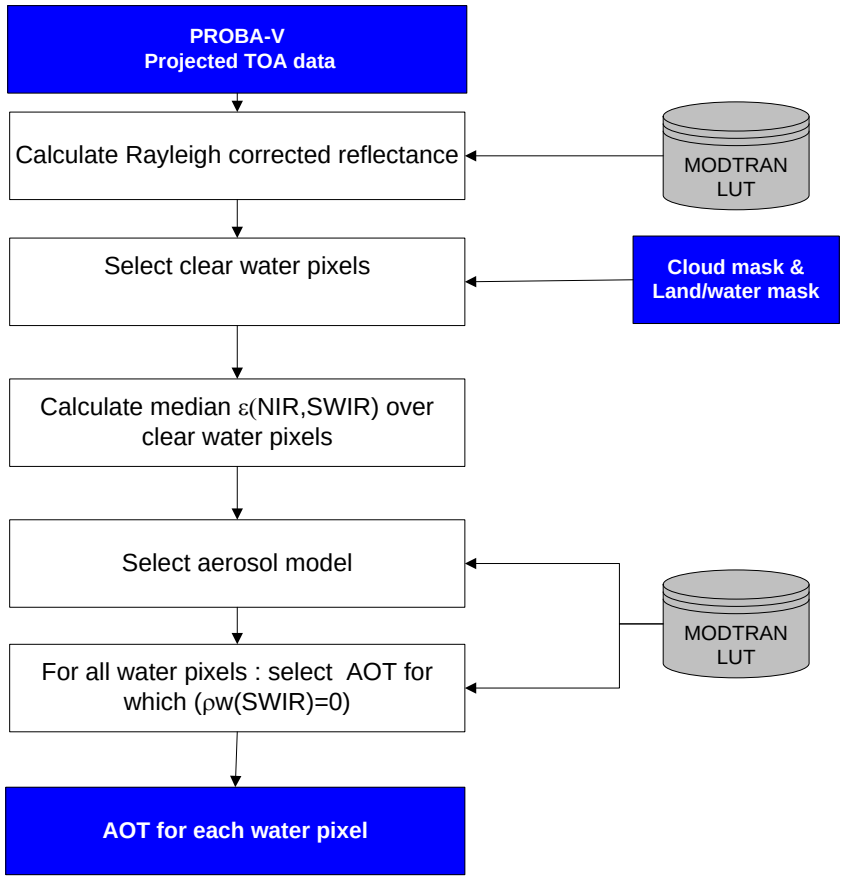

Figure 6. Flowchart SWIR-based AOT retrieval

2.10. APPLICATION OF THE ATMOSPHERIC CORRECTION PARAMETERS

Finally the atmospheric correction parameters stored in the LUT are linearly interpolated on the multiple variables (sun and view angles and AOT) to derive for each pixel the corresponding parameters in order to derive the water leaving radiance reflectance on the basis of equation 2.10 and 2.12.

2.11. SOURCES OF UNCERTAINTY

Here we list the main error sources in the proposed atmospheric correction method. A more detailed error budget will be given in next version of the ATBD in which validation results against Aeronet(-OC) stations for both AOT and water leaving reflectance will be taken into account.

- Error in the aerosol type: Atmospheric correction parameters are only calculated for three types of standard Modtran-5 aerosol models (i.e. Rural, maritime and urban). While for some coastal sites these standard aerosols might represent well the actual aerosol type, the aerosol type for other regions might differ more significantly. In the land based AOT retrieval approach the aerosol model is a priori fixed which might deviate from the selected aerosol model. In the SWIR based aerosol retrieval approach the aerosol type is defined over the offshore clear waters. The aerosol type over the offshore waters might be different from the one over the coastal waters. Furthermore due to low SNR values in SWIR for low radiance targets, discrimination between the three aerosol types might be difficult. According to Vanhellemont and Ruddick (2015) impact on the atmospheric correction of a wrong aerosol type selection is relatively small for turbid waters as the marine reflectance is very strong compared to the aerosol reflectance (Vanhellemont and Ruddick, 2015).
- Error in the AOT retrieval : According to Guanter et al. (2008) +/- 0.03 can be assumed as the intrinsic error associated to AOT retrievals with the land based AOT retrieval approach. Further uncertainties arises from the spatial extension of the AOT retrieved from nearby land to the coastal water due to possible spatial inhomogeneity of the AOT. For the SWIR based AOT retrieval approach the pixel dependent noise in the SWIR band will directly influence the AOT retrieval.
- Water vapor : An error in the water vapor of about 20 % is typically assumed. An error in the water vapor gaseous transmittance will have a direct effect on the RED, NIR and SWIR band reflectance. Following equation (2.14) with Table 1 as input a 20 % error in the water vapor gives in average a 0.06 %, 0.4% and 0.01 % error in respectively the RED, NIR and SWIR band reflectance. Except for the NIR band the impact is therefore negligible.
- Ozone: An error in the ozone amount of about 5 % is typically assumed. An error in the ozone gaseous transmittance will have a direct effect on the BLUE and RED band reflectance. Following equation (2.14) with Table 1 as input a 5 % error in the ozone content gives in average a 0.01 % and 0.06 % error in respectively the BLUE and RED band reflectance. The impact can be considered negligible.
- Sensor noise and calibration error: The direct impact of sensor noise is quantified following the approach schematically given in Figure 7. In-situ water reflectance spectra, acquired in the frame of the SeaSWIR project over turbid waters, are transformed to at-sensor level radiance spectra using the MODTRAN-5 radiative transfer code and spectrally resampled to the PROBA-V band. Next, different levels of noise are added to the simulated at-sensor radiance spectra. We added three levels of the correlated noise with 316, 100 and 31 signal-to noise ratio (SNR). The latter two noise levels represent the SNR of PROBA-V sensor for low (e.g. turbid waters) to extremely low (e.g. clear waters) radiances for unbinned pixels. A SNR of 316 is representative for binned pixels. All noises were generated from Gaussian (white) noise by low-pass filtering with a normalized cut-off frequency of $5\pi/L$ for each SNR. Next , the TOA reflectance spectra are be converted back to surface reflectance by performing the atmospheric correction. In order not to add uncertainty from the atmospheric condition parameters; we used the same atmospheric condition parameters which were used to convert the spectra into at-sensor radiance. The resulting reflectance spectra are then compared against the input spectra to assess the impact of the sensor noise. The mean relative (in %) and absolute errors are given in Table 4 for the VNIR bands.

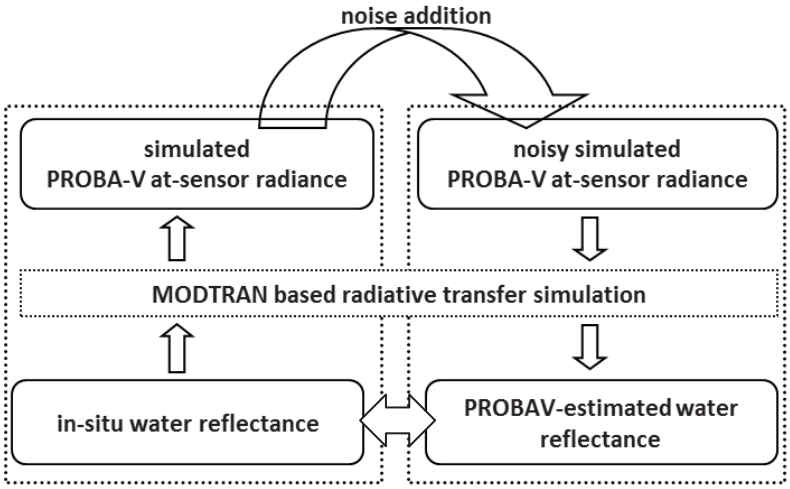

Figure 7. Schematic overview of approach to assess impact of sensor noise on retrieved reflectance spectra

Table 4. Atmospheric correction error due to sensor noise

	SNR =31			SNR =100			SNR=314		
	BLUE	RED	NIR	BLUE	RED	NIR	BLUE	RED	NIR
Mean Rel. Error (%)	9.5066	5.0042	13.6849	4.3911	1.5241	3.9105	0.9427	0.4841	1.0523
Stdev (%)	8.5251	4.2695	12.4695	3.2552	1.3382	3.6345	0.8176	0.4274	1.0166
Mean abs. Error	0.0044	0.0048	0.0079	0.0020	0.0015	0.0022	0.0004	0.0005	0.0006
Stdev	0.0035	0.0034	0.0059	0.0013	0.0010	0.0015	0.0003	0.0003	0.0004

2.12. VALIDATION WITH AERONET-OC

To validate the A/C method a so called "direct validation approach" will be used. In the direct validation approach, the retrieved PROBA-V water leaving radiance reflectance is compared with the corresponding in-situ AERONET-OC measurements (see also test data documentation). For this the normalized water leaving radiances ($L_{wn} = \pi . \rho_w . F_0$), measured by AERONET-OC CIMEL instruments is converted to water leaving radiance reflectance (ρ_w).

As can be seen in Figure 8 PROBA-V spectral bands are much broader than the AERONET-OC spectral bands, which complicates the "direct" comparison. In order to take into account the difference in center wavelength and band width "a spectral shift" correction should be applied before performing the "direct" comparison.

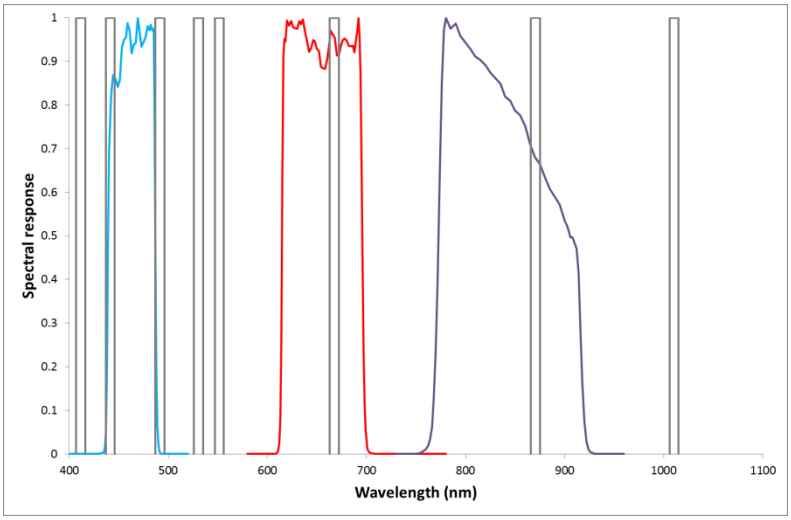

Figure 8. Comparison AERONET-OC (in grey) and PROBA-V spectral bands

To determine the spectral shift correction hyperspectral in-situ measured ρ_w spectra acquired from the Scheldt, La Plata and Gironde estuary in the frame of the SeaSWIR project and ρ_w spectra from the North Sea from the Coastcolour dataset (Nechad et al., 2015) are used (Figure 9). Please note that the Coastcolour North Sea dataset only partly covers the PROBA-V NIR band and can therefore not be used for the calculation of the spectral shift correction factor for the NIR band. In addition to the in-situ hyperspectral spectra, simulated NIR spectra will be used. These spectra are calculated assuming an invariant shape of the water reflectance in the NIR (Figure 10). This invariant shape was defined by Ruddick et al. (2006) by normalization at 780 nm and referred to as NIR similarity spectrum.

These in-situ and hyperspectral datasets are spectrally resampled to both the PROBA-V and the AERONET-OC spectral bands. Next, a regression analysis is performed between the resampled ρ_w data for the corresponding bands in order to define the "spectral shift" correction to be applied to the real data.

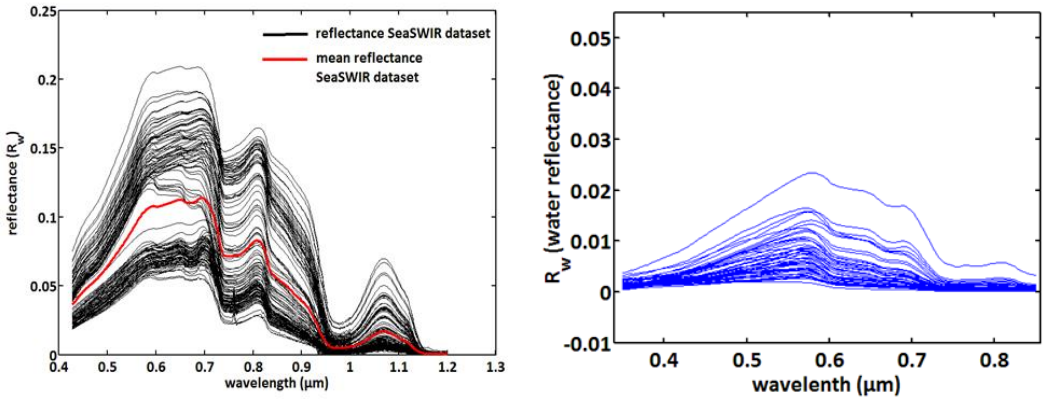

Figure 9. Hyperspectral in-situ measured ρ_w spectra used to determine the spectral shift correction between AERONET-OC and PROBA-V spectral bands. Left: ρ_w spectra from the Scheldt, La Plata and Gironde estuary acquired in the frame of the SeaSWIR project. Right: ρ_w spectra from the North Sea from the Coastcolour dataset.

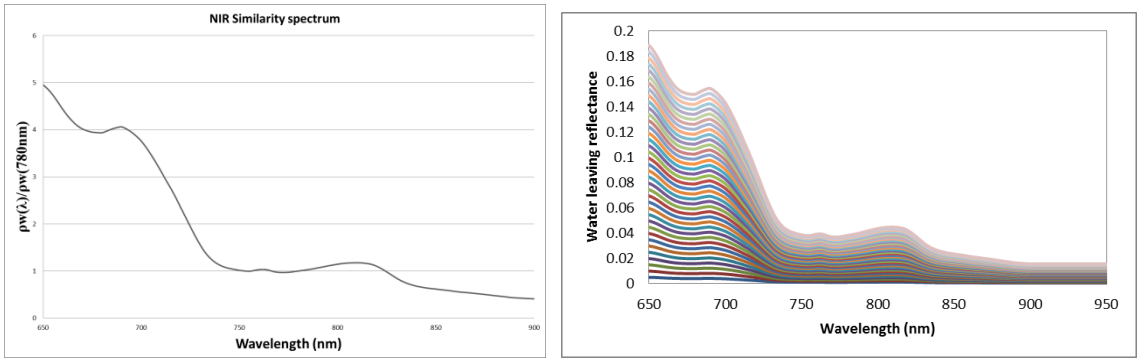

Figure 10. Left: NIR similarity spectrum (reproduced after Ruddick et al. (2006)). Right: Simulated hyperspectral spectra assuming an invariant shape determined by the NIR similarity spectrum

In Figure 11, Figure 12 and Figure 13 the spectral shift correction functions based on respectively SeaSWIR, Coastcolour and Simulated datasets are given. In Figure 14 spectral shift correction functions based on all the datasets together is given. For PROBA-V BLUE and RED band a single, site independent, spectral shift correction function can be found with a R^2 better than 0.99 (Figure 13). For the NIR band significant variability seems to exist between sites (Figure 11). Furthermore the spectral correction function based on the synthetic spectra seem to deviate from the function based on the in-situ datasets.

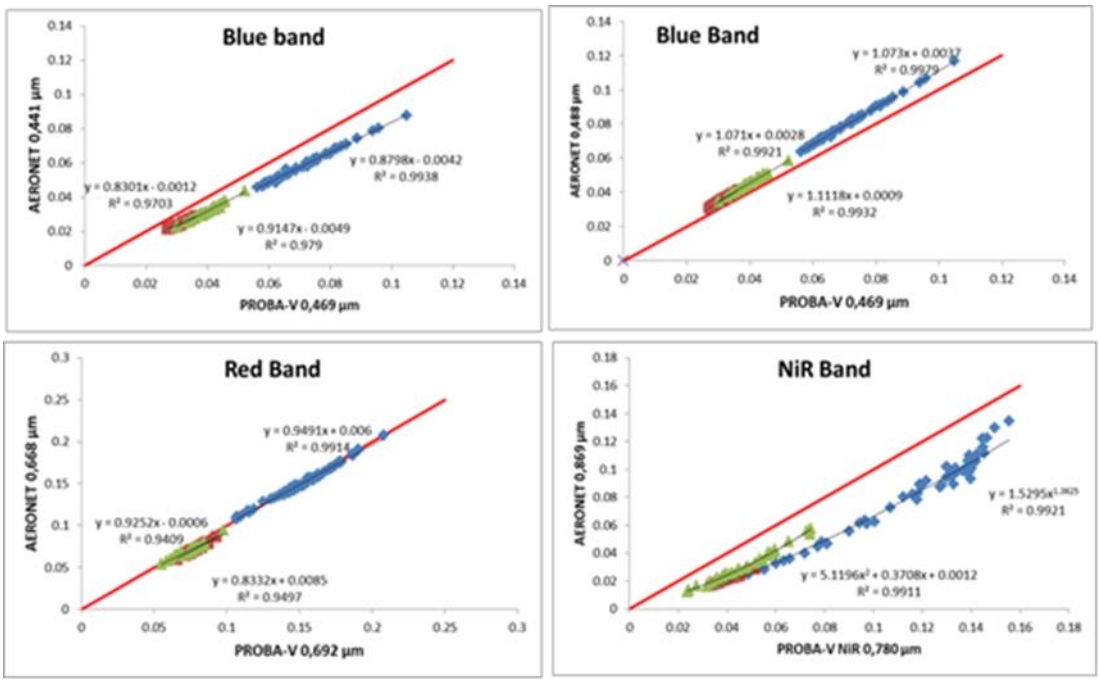

Figure 11. Spectral shift correction functions for BLUE, RED and NIR bands based on SeaSWIR dataset

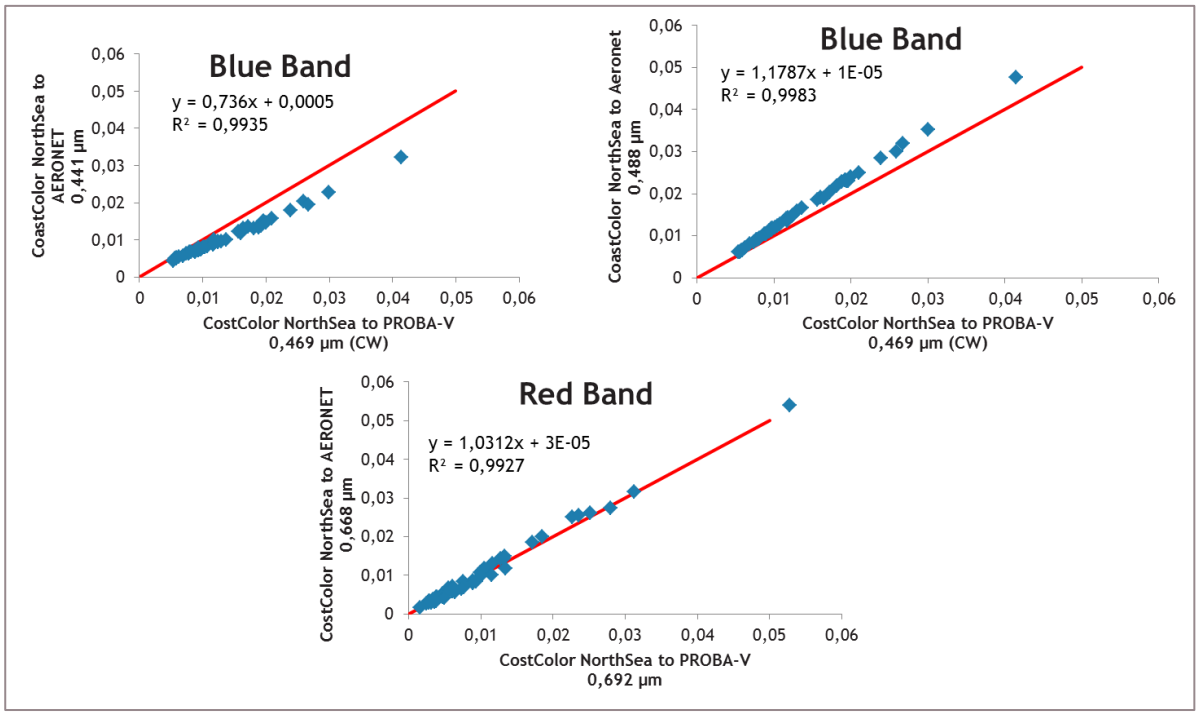

Figure 12. Spectral shift correction functions for BLUE and RED based on Coastcolour dataset from the North Sea

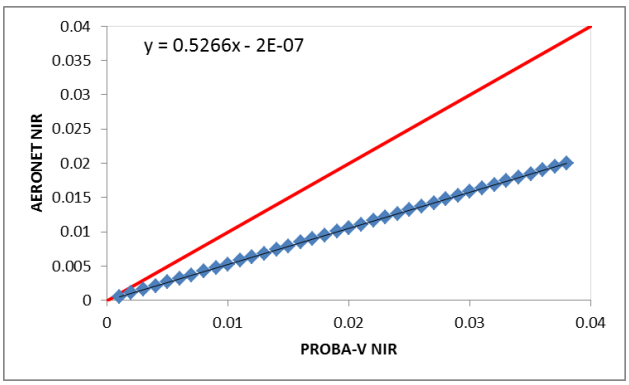

Figure 13. Spectral shift correction functions for NIR band based on simulated dataset

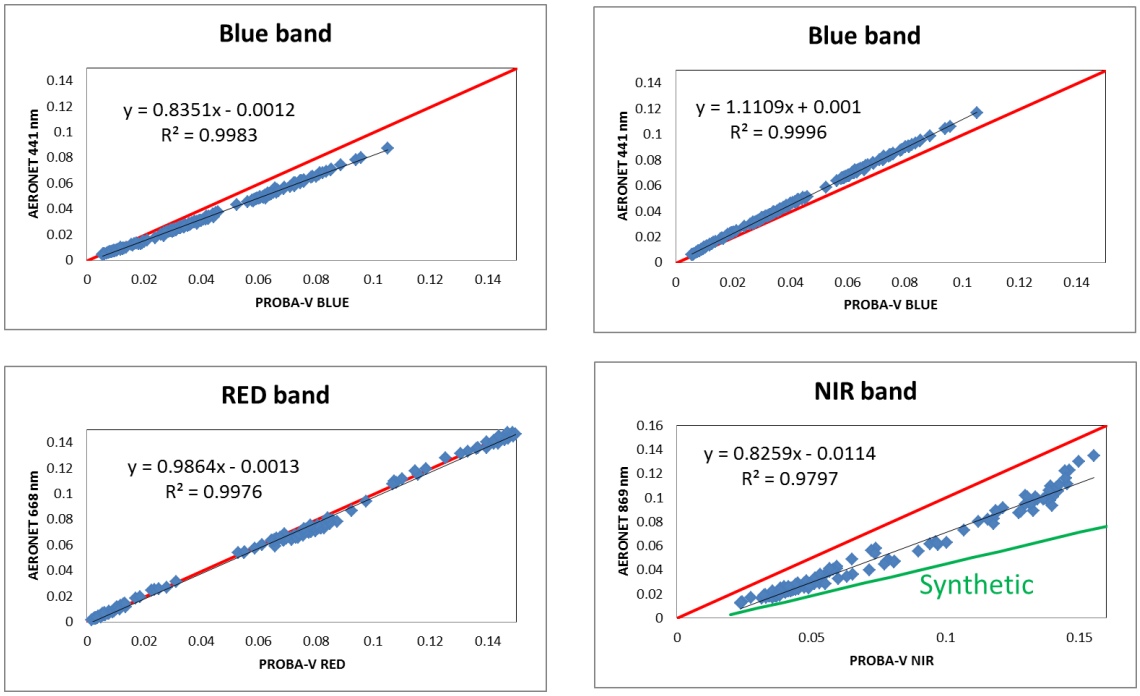

Figure 14. Spectral shift correction functions for BLUE and RED based on Coastcolour North Sea and SeaSWIR dataset and for NIR band based on SeaSWIR dataset with synthetic results superimposed.

CHAPTER 3 TSM/TURBIDITY ALGORITHMS

3.1. REGIONAL SINGLE BAND TSM ALGORITHM

3.1.1. THEORETICAL BASIS

The Nechad et al. (2010) semi-analytical single band algorithm relates the water leaving reflectance in a single band to the TSM concentration as follows :

$$\mathrm{TSM} = \frac{\mathrm{A}^{\rho}\cdot\rho_{\mathrm{w}}(\lambda)}{\left(1-\frac{\rho_{\mathrm{w}}(\lambda)}{\mathrm{C}^{\rho}}\right)} \tag{3.1}$$

where the calibration parameters A^{ρ} (in $\mathrm{g}\cdot\mathrm{cm}^{-3}$) and the asymptotic limit C^{ρ} (dimensionless) are given by :

$$\mathrm{A}^{\rho} = \frac{\mathrm{A}}{\gamma} \tag{3.2}$$

$$\mathrm{C}^{\rho} = \frac{\gamma\cdot\mathrm{C}}{(1+\mathrm{C})} \tag{3.3}$$

With

A the ratio of non-algal particulate absorption ($\mathrm{a_{np}}$) to the specific particulate backscattering coefficient ($\mathrm{b^{*}_{bp}}$) :

$$\mathrm{A} = \frac{\mathrm{a_{np}}}{\mathrm{b^{*}_{bp}}} \tag{3.4}$$

C the ratio of the specific particulate backscattering and the specific particulate absorption ($\mathrm{a^{*}_{p}}$):

$$\mathrm{C} = \frac{\mathrm{b^{*}_{bp}}}{\mathrm{a^{*}_{p}}} \tag{3.5}$$

and

$$\gamma = \pi.R.f'/Q \tag{3.6}$$

where f'/Q is the bi-directionality factor. f'/Q is set to a constant value of 0.13 as derived by Loisel and Morel (2001) for sediment-dominated waters. R represents reflection and refraction at the sea surface. Following Morel and Gentilli (1996) R is set to 0.529. This results in a γ of 0.216.

The relationship between TSM and water-leaving reflectance depends on site specific particulate backscattering and absorption properties which prevents the global usage of the relationship. It should be noted that in the linear part of the algorithm the relationship (3.1) is rather insensitive to errors in the C^{ρ} coefficient. Therefore the C^{ρ} values computed in Nechad et al. (2010) based on standard inherent optical properties (IOPs) can be used as long as the asymptotic limit is avoided. Site specific recalibration of the C^{ρ} is not necessary. Therefore only the A^{ρ} coefficient requires site-specific calibration.

3.1.2. PROBA-V CALIBRATION COEFFICIENTS FOR THE NORTH SEA

In Nechad et al. (2010) the A^{ρ} coefficient was calibrated based on a large set of in-situ hyperspectral water-leaving reflectance spectra and corresponding TSM values, collected from the Southern North Sea. A non-linear regression analysis is used to find the optimal parameters A^{ρ} that gives for equation (3.1) the best fit to TSM and ρ_w. A table of the retrieved A^{ρ} and the computed C^{ρ} coefficients are given in Nechad et al. (2010) at 2.5 nm resolution.

The spectrally resampled A^{ρ} and C^{ρ} values for the PROBA-V RED and NIR bands are given in Table 5. In Figure 15 these values are used to plot the variation in the water leaving radiance reflectance in PROBA-V RED and NIR bands with respect to a change of TSM concentration.

Table 5. Calibration coefficients A^{ρ} and C^{ρ} for the PROBA-V RED and NIR bands (resampled from Nechad et al. (2010)) for retrieval of TSM following eq. 3.1

PROBA-V band	A^{ρ}	C^{ρ}
RED	309	0.168
NIR	2193	0.209

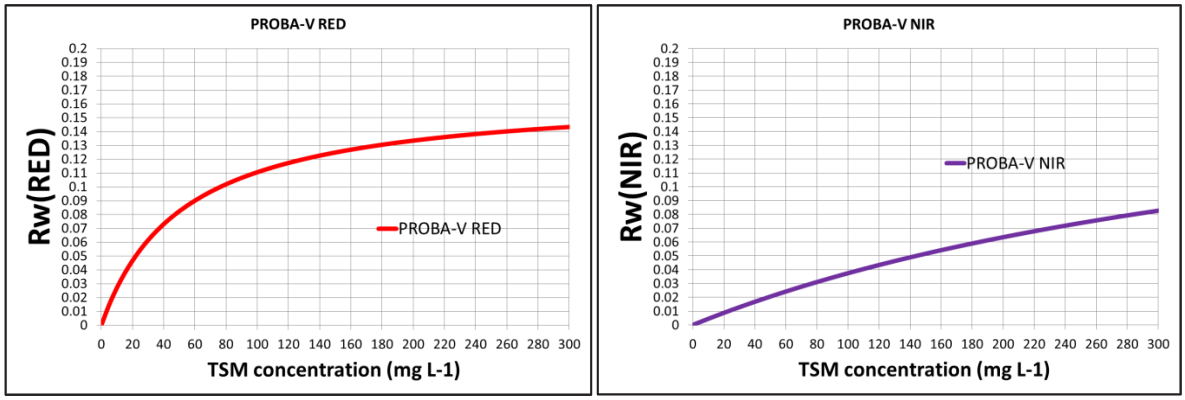

Figure 15. PROBA-V water leaving reflectance in RED and NIR bands in function of the TSM concentration, following the Nechad et al. (2010) algorithm

The reflectance in the RED band is very sensitive to low and medium TSM concentrations where the relationship is approximately linear but saturates at higher TSM concentrations. While the NIR is less sensitive to low—medium TSM concentrations, saturation seems to occur only at very high TSM concentrations. Because of the different sensitivity to the level of TSM concentration, wavelength switching TSM algorithms have been proposed by various authors (e.g. Han et al., 2016, Shen et al. (2010), Dogliotti et al. (2015)) based on either TSM or water leaving reflectance thresholds.

To identify the reflectance at which switching should take place, the relationship between the RED and NIR PROBA-V band from the Nechad et al. (2010) algorithm are modelled following equation (3.1) with calibration coefficients taken from Table 5. A logarithmic regression curve (red line in Figure 16). The first derivative is calculated which is a measure of the rate at which the value y (i.e. RED reflectance) of the function changes with respect to the change of the variable x (i.e. NIR reflectance). In Figure 16 this derivative is shown as the slope of the tangent line (red dotted line) of the regression curve. Once this slope or derivative reaches the value 1 (red square in Figure 16),

the change in NIR reflectance will be larger than the change in RED reflectance. This is exactly the point where we want to switch between the Red and the NIR PROBA-V band in order to have the best sensitivity. It corresponds to a RED reflectance of 0.11. To obtain smooth transitions in the processed TSM images a switching window is proposed between $\rho_w(RED)$= 0.10 and $\rho_w(RED)$ = 0.12. These correspond to TSM values of 76 and 129 mg L-1.

In summary:

- For $\rho_w(RED)$< 0.10 use TSM derived on the basis of the RED band
- For $\rho_w(RED)$ > 0.12 use TSM derived on the basis of the NIR band
- For 0.10 < $\rho_w(RED)$< 0.12 perform merging :

$$TSM = (1-w) * TSM(RED) + w * TSM(NIR) \quad (3.7)$$

Where w changes linearly from 0 at $\rho_w(RED)$=0.10 to 1 at $\rho_w(RED)$=0.12.

These results show that switching will only occur in very turbid waters and will not occur regularly in the North Sea waters. In some other publications switching was proposed at lower reflectances (e.g. Dogliotti et al. (2015) proposed switching between the MODIS 645 nm and 859nm bands at a $\rho_w(645)$ between 0.05 and 0.07). The broad NIR band of PROBA-V prohibits in this case switching at these lower reflectances.

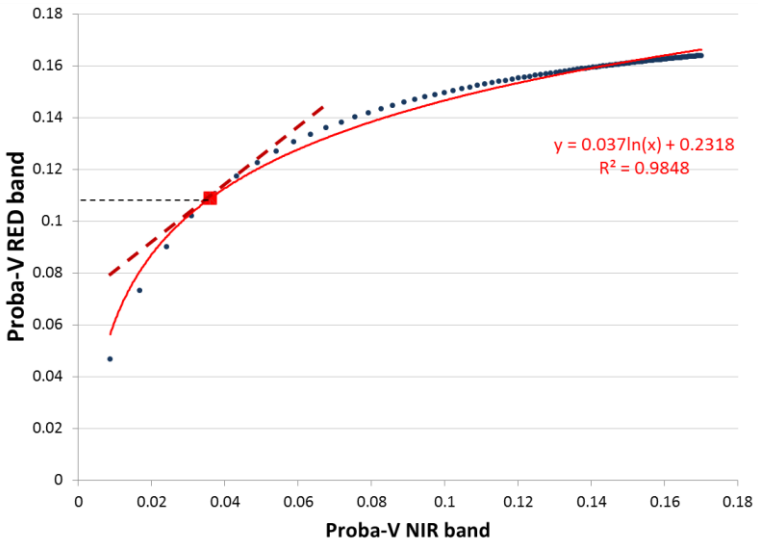

Figure 16. Relationship between PROBA-V RED and NIR reflectance following TSM equation (3.1) with calibration coefficients taken from Table 5. Red line: logarithmic regression curve.

3.1.3. SITE SPECIFIC RECALIBRATION OF THE ALGORITHM

Nechad et al. (2010) showed that results are not very sensitive to C^ρ, thus, as long as the asymptotic limit is avoided recalibration of the C^ρ is not necessary and only the A^ρ coefficient requires recalibration .

Two approaches can be followed for the site specific recalibration of the A^ρ coefficient.

A first option is to recalibrate the A^ρ coefficient based on site specific data of inherent optical properties as the non-algal particulate absorption (a_{np}) and the specific particulate backscattering coefficient b^*_{bp}. Variation in space and time of the non-algal particulate absorption (a_{np}) is

assumed negligible outside strong CDOM absorption spectral regions. Therefore it is mainly the specific particulate backscattering coefficient b_{bp}^{*} which will be critical parameter. b_{bp}^{*} can be determined in-situ through the measurement of both TSM and the backscattering measured in-situ with a backscattering sensor (such as for example a HydroScat-6).

The second option is to use in-situ databases of locally measured hyperspectral ρ_w data and corresponding TSM values. The hyperspectral R_w data are convolved with sensor spectral response curve. Through a non-linear regression analysis the optimal site specific A^{ρ} can be derived. The non-linear regression analysis is best performed in a logarithmic space. The sum of error squares (SSE) and the coefficient of multiple determination R^2 in log-transformation are given by

$$SSE_{log} = \sum_{i=1}^{N}\left[\log(TSM_i) - \log\left(\widehat{TSM_i}\right)\right]^2 \quad (3.8)$$

$$R^2 = 1 - \frac{SSE_{log}}{\sum_{i=1}^{N}\left[\log(TSM_i) - \sum_{j=1}^{N}\log(TSM_j)/N\right]^2} \quad (3.9)$$

with TSM_i the in-situ measured TSM values and TSM_i the model estimates.

The coefficient A^{ρ}that minimizes SSE_{log}, corresponding to the highest R^2 is selected as optimal site specific calibration coefficient.

3.1.4. ERROR BUDGET

→ Literature

According to Nechad et al. (2010) the algorithm is most suitable for moderate turbid waters (TSM > 10 gm^{-3}). The authors found relative errors less than 30 % in the TSM estimates when applying equation 3.1 to seaborne reflectance measurements from the North Sea, i.e. the same site as where the algorithm was calibrated for initially. When applied to MERIS and MODIS data from the North Sea the relative errors were respectively 33 % and 40 % for TSM > 2 gm^{-3}; higher relative errors were found in clearer waters. Satellite derived TSM concentrations exhibit larger relative errors due to additional atmospheric correction errors; which will be most significant for clear waters.

→ PROBA-V

A preliminary testing of the performance of the TSM algorithm for PROBA-V is performed through application of the algorithm to existing in-situ datasets containing simultaneous measurements of above-water remote sensing reflectance and TSM concentrations. For this we used both the CoastColour Round Robin in-situ database for the North Sea region (Nechad et al., 2015) and the the SEASWIR dataset (Knaeps et al, 2015) containing data from the Scheldt, Gironde and La Plata estuaries. For more details with respect to these datasets we refer to test dataset documentation The above-water remote sensing reflectance are spectrally resampled to the PROBA-V RED and NIR spectral bands prior to the application of the TSM algorithm (3.1) using the PROBA-V specific calibration coefficients given in Table 5 .

A scatterplot of the retrieved TSM values versus the measured TSM values are given in Figure 17 and Figure 18 for respectively the North Sea CoastColour and the SEASWIR dataset is given in Figure 22. For the North Sea dataset the TSM algorithm (3.1) gives similar errors (between 37-40 %) for both the RED and the NIR band , but when using RED band the TSM concentration is underestimated, while with the NIR band it is overestimated. It should be noted that Nechad et al.

(2010) claimed that the algorithm is mainly suitable for moderate turbid waters (TSM > 10 gm^{-3}) whereas the Coastcolour dataset is dominated with measurements with TSM well below 10 gm^{-3}

More validation will be performed in the next phase of project using real PROBA-V data

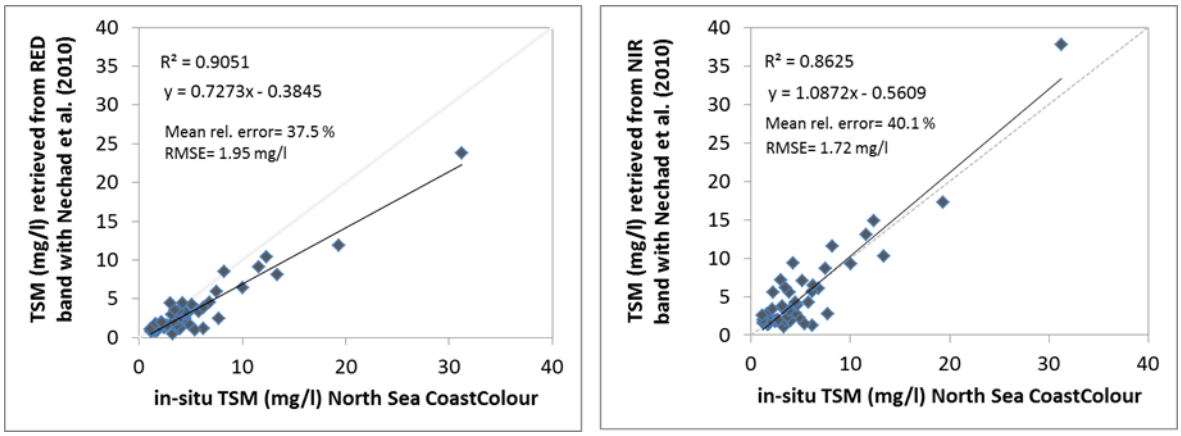

Figure 17.TSM(mg/l) derived from the CoastColour in-situ reflectance dataset for the North-Sea versus the in-situ TSM, retrieved from reflectance resampled to the PROBA-V RED (left) and NIR (right) bands.

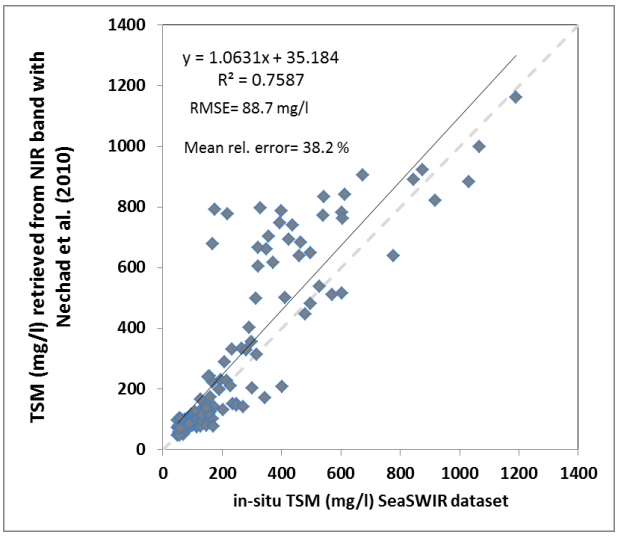

Figure 18.TSM (mg/l) derived from the SeaSWIR in-situ reflectance dataset (from Scheldt, Gironde and La Plata estuaries) versus the in-situ TSM, retrieved from reflectance resampled to the PROBA-V NIR band.

3.2. GLOBAL TURBIDITY ALGORITHM

3.2.1. THEORETICAL BASIS

Turbidity of a water sample is an optical measure of the extent to which the intensity of light passing through water is reduced by the particles in the water. Turbidity is therefore strongly related to TSM. Turbidity can be expressed in various units, such as Formazin Turbidity Unit or FTU, Nephelometric Turbidity Unit or NTU. Turbidity is listed by the European Union as one of the prime

water quality parameters to be measured regularly. Due to the fact that turbidity is an optical property, it is more related to reflectance through the backscattering than TSM.

The one-band turbidity algorithm originally developed by Nechad et al. (2009) is proposed. The algorithm relates turbidity (T) to the water reflectance ρ_w through

$$T = \frac{A_T^{\rho} \cdot \rho_w(\lambda)}{\left(1 - \frac{\rho_w(\lambda)}{C_T^{\rho}}\right)} \quad (3.10)$$

Where A_T^{ρ} and C_T^{ρ} are wavelength dependent calibration coefficients.

As can be seen this equation has a similar form as the TSM algorithm (eq. 3.1) , but instead of using a backscattering to TSM relationship, a backscattering to Turbidity relationship (T) is adapted. The turbidity-specific particulate absorption and backscattering is defined as

$$a_{pT}^{*} = \frac{a_p}{T}, b_{bpT}^{*} = \frac{b_{bp}}{T} \quad (3.11)$$

A_T^{ρ} is related to the inherent optical properties by

$$A_T^{\rho} = \frac{a_{np}}{\gamma . b_{bpT}^{*}} \quad (3.12)$$

with γ equal to 0.216 (as given in eq. 3.6).

The C_T^{ρ} is the asymptotic limit of eq. 3.10 and is given by

$$C_T^{\rho} = \gamma \frac{b_{bpT}^{*}}{a_{pT}^{*} + b_{bpT}^{*}} \quad (3.13)$$

In the linear region where $\rho_w(\lambda) << C_T^{\rho}$ the C_T^{ρ} has a very minor impact on the retrieved turbidity. Therefore an error in C_T^{ρ} will have a negligible impact in the linear region. C_T^{ρ} is calculated using standard inherent optical properties. The A_T^{ρ} coefficient was obtained by a non-linear regression analysis using in situ measurements of T an ρ_w and tabulated for every 2.5 nm in Nechad et al. (2009) and later improved in Dogliotti et aL (2011) (only for MODIS bands) based on an extended set of in-situ data. In Table 6 the C_T^{ρ} and A_T^{ρ} for the PROBA-V RED and NIR bands are given. For the calculation of A_T^{ρ} (NIR) the tabulated values in Nechad et al. (2009) are spectrally resampled and the retrieved value is adjusted considering the percentage change proposed by Dogliotti et aL (2011) with respect to the Nechad et al. (2009) values.

Table 6. Calibration coefficients A_T^{ρ} and C_T^{ρ} for the PROBA-V RED and NIR bands for retrieval of Turbidity following eq. 3.10

PROBA-V band	A_T^{ρ}	C_T^{ρ}
RED	237.891	0.168
NIR	2535.41	0.209

Similarly for turbidity, the modeled regression curve is shown in Figure 19. The point where the slope of the tangent line is 1 corresponds to $\rho_w(RED)$= 0,1 or a turbidity of 60 FNU.

A switching window can be defined between $\rho_w(RED)$= 0,09 and $\rho_w(RED)$= 0,11, corresponding to 46 and 76 FNU.

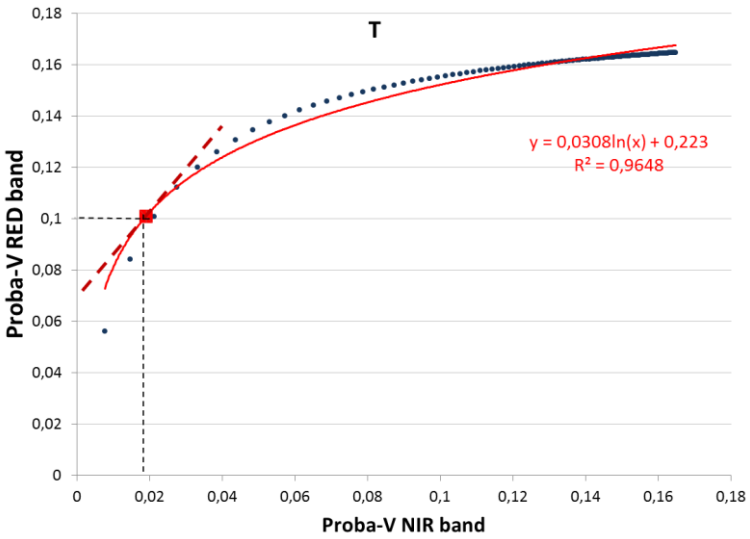

Figure 19. Relationship between PROBA-V RED and NIR reflectance following Turbidity equation (3.1) with calibration coefficients taken from Table 6. Red line: logarithmic regression curve

3.2.2. GLOBAL APPLICABILITY OF THE ALGORITHM AND ERROR BUDGET

→ Literature

An assessment of the impact of regional variability of the scattering phase function on the retrieval uncertainty has been performed in Dogliotti et al. (2015) on the basis of radiative transfer calculations. They found that retrieval uncertainty is expected to be less than 6% for very different scattering phase function .

In Dogliotti et al. (2015) the algorithm (3.10) was applied to in-situ measured water leaving reflectance spectra acquired from five different sites, i.e. European and South American coastal and estuarine waters. The turbidity estimates were within 12 and 22 % (depending on the site) of the in-situ measured Turbidity values. Combining all the data, covering a 1.8-988 FNU Turbidity range, a mean relative error of 13.7 % was obtained which is good indication of the global applicability of the Turbidity algorithm for turbid waters with a turbidity within the 1-1000 FNU range.

It should be noted that in the study of Dogliotti et al. (2015) the accuracy of the Turbidity algorithm was only evaluated on in-situ measured reflectance and not on satellite derived reflectance values. Atmospheric correction errors and sensor noise (low signal-to-noise ratio) might reduce the performance of the algorithm. Still various authors have reported successful retrieval of the turbidity when applying the Dogliotti et al. (2015) algorithm to various satellite data: Brando et al. (2015) applied the Dogliotti et al. (2015) turbidity algorithm to Landsat8 images to characterize the turbidity in river plumes in the northern Adriatic Sea. Constantin et al. (2016) used the algorithm to retrieve the turbidity in the Black Sea based on MODIS observations. Unfortunately no accuracy assessment was performed in these studies.

→ **PROBA-V**

A preliminary testing of the performance of the Turbidity algorithm for PROBA-V is performed through application of the algorithm to existing in-situ datasets containing simultaneous measurements of above-water remote sensing reflectance and Turbidity. For this we used the the SEASWIR dataset (Knaeps et al, 2015) containing data from the Scheldt, Gironde and La Plata estuaries. For more details with respect to these datasets we refer to test dataset documentation The above-water remote sensing reflectance are spectrally resampled to the PROBA-V RED and NIR spectral bands prior to the application of the Turbidity algorithm (3.10) using the PROBA-V specific calibration coefficients given in Table 5. A scatterplot of the retrieved Turbidity versus the measured Turbidity is given in Figure 22. Turbidity estimates are in average within 12.6 % with an average RMSE of 35.5 FNU, these numbers are in line with Dogliotti et al. (2015). The performance of the Turbidity algorithm clearly outperforms the TSM algorithm where for the same sites average error of 38.2 % were obtained (see Figure 18). These results suggest that the Turbidity algorithm (3.10) can be used in very different using RED and NIR bands of PROBA-V. However more extensive validation on real PROBA-V data is needed.

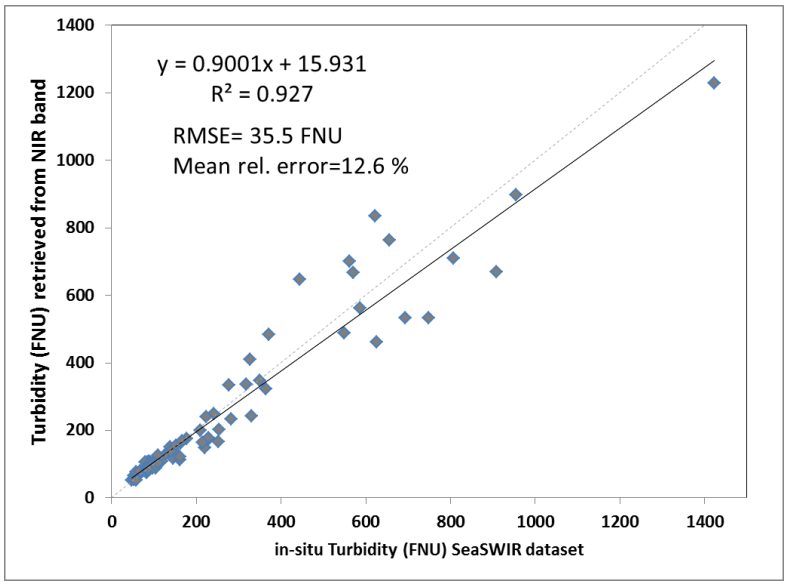

Figure 20.Turbidity (FNU) derived from the SeaSWIR in-situ reflectance dataset (from Scheldt, Gironde and La Plata estuaries) versus the in-situ measured Turbidity, retrieved from reflectance resampled to the PROBA-V NIR band.

3.2.3. LOCAL TURBIDITY-TSM RELATIONSHIPS

In order to retrieve TSM, a regional TSM-turbidity relationship has to be established to convert the turbidity values to TSM concentrations. As discussed further in section 3.2.4 the establishment of this relationship should be best done based on in-situ turbidity measurements performed using a similar type of turbidity meter as used by Dogliotti et al. (2015) and Nechad et al. (2009).

Within the BELSPO funded Proba4Coast project several seaborne campaigns have performed at the Norths Sea (see also test dataset documentation) where both TSM and turbidity was measured. For the turbidity measurements a portable HACH turbidity meter was used (as in Dogliotti et al. (2015) and Nechad et al. (2009)). In Figure 21 the turbidity-TSM relationship is given which can be then later applied to the PROBA-V retrieved turbidity values from the North Sea in order to derive the TSM concentration.

Furthermore water samples from the Scheldt river were collected over the tidal cycle from a fixed pontoon (51° 14'N- 4°23' E) near the city of Antwerp at three different dates. These samples were analyzed in the lab for TSM concentration and turbidity was measured with a portable HACH turbidity meter. In Figure 22 the established turbidity-TSM relationship for the Scheldt is given.

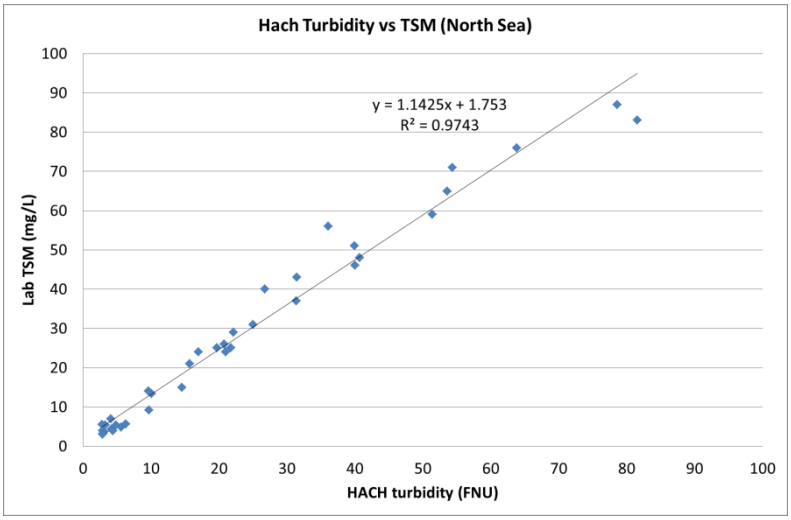

Figure 21. Turbidity-TSM relationship set-up for the North Sea

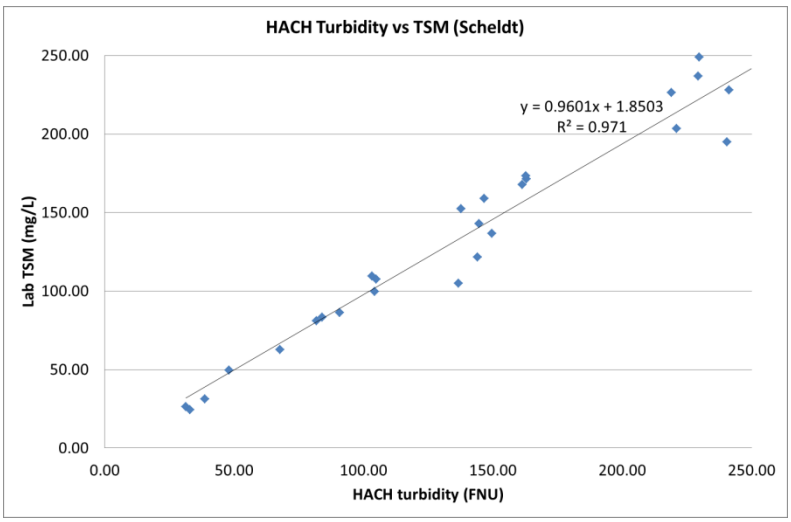

Figure 22. Turbidity-TSM relationship set-up for Scheldt river

3.2.4. TURIBIDITY METERS

In Nechad et al. (2009) and Dogliotti et al. (2015) the Turbidity algorithm was set-up based on Turbidity measured on collected water samples with portable HACH (type 2100P and 2100QIS) turbidity meters. These HACH instruments measure the turbidity on a 10-ml water sample. Portable HACH turbidity meters determine turbidity at 860 nm based on the ratio of 90° (+/- 2.5°) scattered light to the forward transmitted light as compared to the same ratio for a standard suspension of Formazine. This optical measurement technique of Turbidity is in accordance with ISO 1999.

For the validation of the PROBA-V derived Turbidity values in-situ measured turbidity by various instruments will be used (see also test dataset documentation). The instrument type, operation specifications (such as wavelength and angular range) are given in Table 7. All of them are calibrated against formazin standards. However they differ among others in the angle range at which the backscattered light is measured. Therefore although calibrated against the same standard, the response of the different turbidity sensors to the same environmental sample might be different.

According to Neuckermans et al. (2012)the wide solid angle of the CEFAS Seapoint turbidity meters also includes forward scattering and increases the instrument's sensitivity to particle size compared to instruments with narrow solid angles in the back direction such as the HACH 2100P turbidimeter.

Rymszewicz et al. (in review) compared eleven types of commercially available turbidimeters and concluded that they all show very high correlation to the suspended sediment concentration but might provide different measurements of turbidity for the same sample. Within the Highroc project four in situ sensors were tested in different tanks with Formazin in fresh water, Formazin in filtered seawater, River water, kaolin in seawater and different algae concentrations in seawater. In situ turbidity meters had 10 to 25% higher values compared to the HACH turbidity meter.

Therefore only the HACH based Turbidity measurement can be used for direct absolute validation of the PROBA-V derived Turbidity values following equation 3.10 which has been set-up on the basis of HACH Turbidity measurements. In-situ turbidity values from other turbidity sensors can be used for relative validation or , in case, a relationship against HACH turbidity measurements can be established also, for absolute validation.

Table 7. Turbidity meters used in the study: Type and operating specifications

	HACH 2100Qis (VITO)	***OBS-3A***	***OBS 3+ (VLIZ)***	***CEFAS Smartbuoy* Seapoint *turbidity meter***
Operating wavelength	860 nm	850 nm/875 nm	850 ± 5 nm	880 nm
Measurement Method, scattering angle	Side scattering 90 ° Ratio turbidimetric determination using a primary nephelometric light scatter signal (90°) to the transmitted light scatter signal.	OBS sensors detect IR backscattered between 140° and 160°, and where the scattering intensities are nearly constant with the scattering angle	OBS3+ measures turbidity from the relative intensity of light backscattered at angles from 90°to 165°.	records light scattered by suspended particles between 15° to 150°
Instrument type	Hand held portable	In-situ probe	In-situ probe	In-situ probe
unit	FNU (operator choice: NTU or FNU)	NTU	NTU	FNU

3.3. EMPIRICAL NIR-RED BAND RATIO ALGORITHM

3.3.1. THEORETICAL BASIS

Single band algorithms might be sensitive to errors in the atmospheric correction and to the variability in reflectance due to the natural variability in the particle scattering properties. To

overcome this issue, as well as to reduce the impact of atmospheric correction errors, empirical band ratios algorithms have been proposed in the literature (Doxaran et. al., 2010; Tassan, J., 2004). As the backscattering has a relatively flat spectral signature, a ratio is less sensitive to changes in the scattering properties. Doxaran et al. (2003) showed on the basis of in-situ measurements that ratio algorithms reduce the effects of variable sediment types and are also less sensitive to illumination conditions.

Following Doxaran et al. (2002) a NIR/RED band ratio algorithm has typically the following form :

$$\mathrm{TSM} = \mathrm{A}.e^{\left(\frac{B.\rho_w(\mathrm{NIR})}{\rho_w(\mathrm{RED})}\right)} \tag{3.14}$$

With A and B regionally and sensor specific, empirically derived, calibration coefficients.

3.3.2. SITE SPECIFIC CALIBRATION OF THE RATIO ALGORITHM

In order to define the PROBA-V and site specific A and B calibration coefficients for equation 3.14 in-situ datasets containing simultaneous measurements of above-water remote sensing reflectance and TSM concentrations. For this we used both the CoastColour Round Robin in-situ database for the North Sea region (Nechad et al., 2015) and the SEASWIR dataset (Knaeps et al, 2015) containing data from the Scheldt, Gironde and La Plata estuaries. Water leaving reflectance spectra are spectrally resampled to the PROBA-V RED and NIR spectral bands before performing the regression of NIR/RED against TSM following equation 3.14. The regression plots for Gironde, La Plata, Scheldt and North Sea are given in Figure 23, Figure 24, Figure 25 and Figure 26, respectively.

For Gironde and Scheldt river with high TSM concentrations, respectively between 86 – 1190 mg/l and between 50-402 mg/l, a very correlation is found between the NIR/RED ratio and the TSM concentration with R^2 values of respectively 0.87 and 0.88.

For the La Plata dataset, with TSM varying between 48.3 and 110 mg/l, the correlation between the NIR/RED ratio and the TSM is much lower (R^2 of 0.16). For the North Sea dataset, with TSM concentrations between 1 and 31 mg/l, almost no correlation could be found (R^2 of 0.05). The correlation significantly improved when removing all observations with TSM less than 6.5 mg/l. The high scattering in the results at low concentrations is mainly caused by the high noise in the NIR reflectance for low values. It should be noted that for real PROBA-V data the noise present in the data will even be larger than for the in-situ data (due to SNR issues for low radiances) which will increase the scattering in the results.

All these plots suggest that NIR/RED band ratio algorithms are mainly suitable for very turbid waters (TSM > 100 mg/l) and should not be applied to more clear waters.

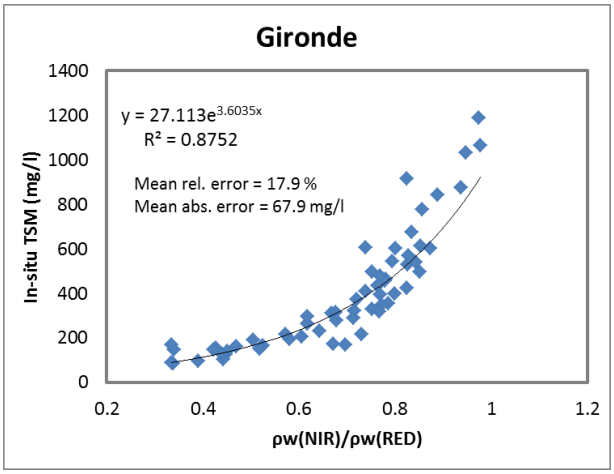

Figure 23. PROBA-V NIR-RED ratio algorithm for the Gironde river (determined based on the in-situ SeaSWIR dataset)

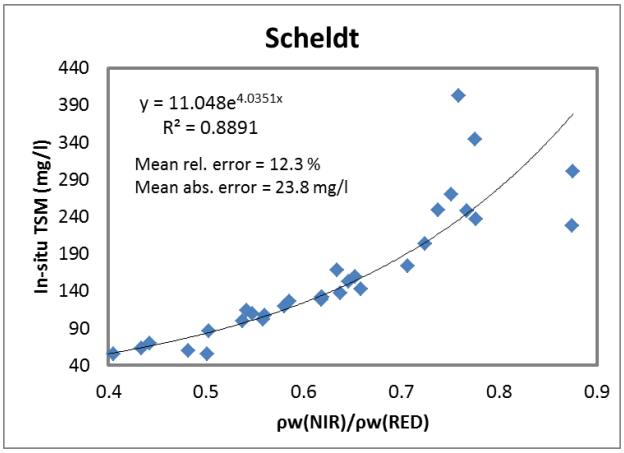

Figure 24. PROBA-V NIR-RED ratio algorithm for the Scheldt river (determined based on the in-situ SeaSWIR dataset)

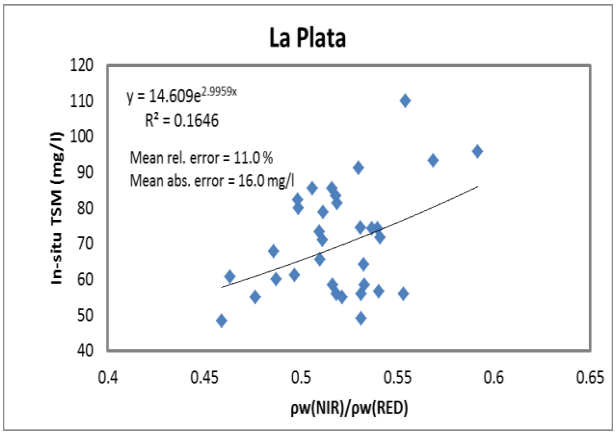

Figure 25. PROBA-V NIR-RED ratio algorithm for La Plata river(determined based on the in-situ SeaSWIR dataset)

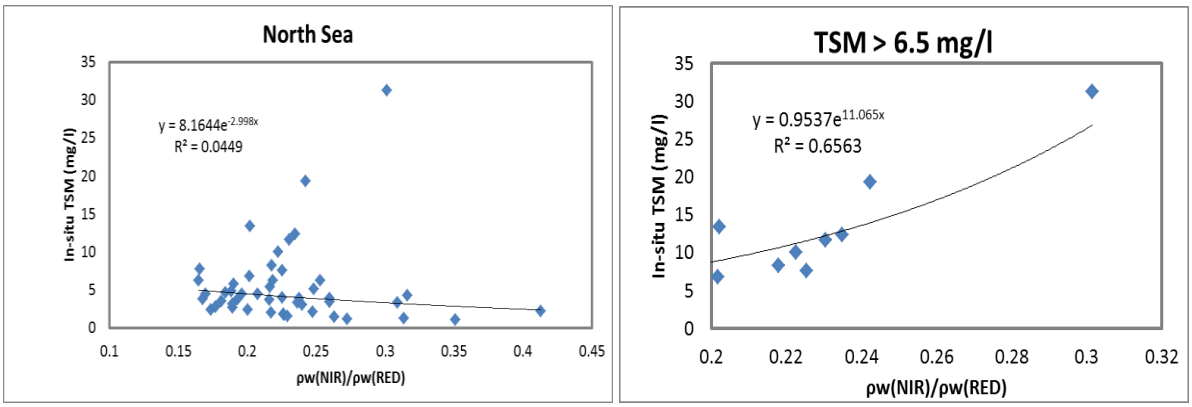

Figure 26. PROBA-V NIR-RED ratio algorithm for the North Sea (determined based on the in-situ Coastcolour dataset). Left : whole dataset. Right: dataset limited to TSM concentrations larger than 6.5 mg/l

CHAPTER 4 IODD

4.1. INTRODUCTION

In this chapter the input and output data for both the atmospheric correction and TSM/Turbidity prototype workflows is described. As both workflows are still under development only a preliminary description is currently given. A more detailed description will be provided with the delivery of the respective prototypes.

4.2. ATMOSPHERIC CORRECTION

4.2.1. INPUT DATA

→ Image data

The atmospheric correction starts from projected PROBA-V TOA data. These can be either S1 TOA 100 m products or the L2A products which will be made available in the reprocessed collection.

From the S1 TOA or L2A data, the following data are used:

- TOA reflectance of BLUE, RED, NIR and SWIR bands
- SZA, VZA, VAA and SAA
- Status Map (SM)
- Date of acquisition

→ Meteo data

- Total column Ozone in units of cm/atm
- Total column water vapor (in kg/m²)
- Optionally, wind speed (ws) at the sea level. This can be calculated from 10 meter U wind component (units: m / s) (ws_U) and 10 meter V wind component (units: m / s) from the ECMWF ERA Interim archive with ws= sqrt(ws_U²+ ws_V²)

→ SMAC coefficients

Pre-calculated coefficients for each spectral band for the exponential variation of the gaseous transmittance with airmass and gaseous amount (SMAC coefficients) for ozone and water: a_{gas}^{k} , n_{gas}^{k} .

→ LUT

Pre-calculated MODTRAN-5 LUTs following the specifications given in 2.3.

4.2.2. OUTPUT DATA

- Image data (ENVI or GEOTIFF format) with the water-leaving reflectance for BLUE, RED, NIR (and SWIR) bands.
- Image data (ENVI or GEOTIFF format) with the retrieved AOT value for every pixel (in case of land based AOT retrieval approach) or for every water pixel (in case of the SWIR black pixel approach)
- ASCII file with $\epsilon^{NIR,SWIR}$ (median, stdev, mean,…) (only for SWIR black pixel approach)

4.3. TSM/TURBIDITY ALGORITHM

4.3.1. INPUT DATA

→ Image data

Image data (ENVI or GEOTIFF format) with the water-leaving reflectance for BLUE, RED, NIR (and SWIR) bands (= output of the atmospheric correction step).

→ Calibration coefficients algorithms

- Single Band TSM Algorithm :
    - Regional (site dependent) Calibration coefficients A^{ρ} and C^{ρ} for the PROBA-V RED and NIR bands
    - Wavelength switching threshold for $\rho_w(RED)$
- Single Band Turbidity Algorithm:
    - Calibration coefficients A_T^{ρ} and C_T^{ρ} for the PROBA-V RED and NIR bands
    - Wavelength switching threshold for $\rho_w(RED)$
    - Optionally for deriving TSM from Turbidity: regional TSM-T calibration coefficients
- Empirical RED-NIR band ratio algorithm
    - Regional A and B calibration coefficients

4.3.2. OUTPUT DATA

- Image data (ENVI or GEOTIFF format) with TSM (units: mg/l) or Turbidity (units: FNU) value for each water pixel.

LITERATURE

Arabi, B.; Salama, M.S.; Wernand, M.R.; Verhoef, W. MOD2SEA: A Coupled Atmosphere-Hydro-Optical Model for the Retrieval of Chlorophyll-a from Remote Sensing Observations in Complex Turbid Waters. Remote Sens. 2016, 8, 722.

Berk, A., G.P. Anderson, P.K. Acharya, L.S. Bernstein, L. Muratov, J. Lee, M. Fox, S.M. Adler-Golden, J.H. Chetwynd, M.L. Hoke, R.B Lockwood, J.A. Gardner, T.W. Cooley, C.C. Borel, P.E. Lewis and E.P. Shettle, "MODTRAN5: 2006 Update," Proc. SPIE, Vol. 6233, 62331F, 2006.

Brando, VE and Dekker, AG, 2003. Satellite hyperspectral remote sensing for estimating estuarine and coastal water quality. IEEE Transactions on Geoscience and Remote Sensing, 41: 1378–1387.

Brando, V. E. and Braga, F. and Zaggia, L. and Giardino, C. and Bresciani, M. and Matta, E. and Bellafiore, D. and Ferrarin, C. and Maicu, F. and Benetazzo, A. and Bonaldo, D. and Falcieri, F. M. and Coluccelli, A. and Russo, A. and Carniel, S., 2015. High-resolution satellite turbidity and sea surface temperature observations of river plume interactions during a significant flood event. Ocean Science, 11(6): 909-920.

Campbell, G., Phinn, S.R., Dekker, A.G., Brando, V.E., 2011. Remote sensing of water quality in an Australian tropical freshwater impoundment using matrix inversion and MERIS images, Remote Sensing of Environment, 115(9): 2402-2414

Chandrasekhar, S., 1960. Radiative Transfer. Dover, New York.

De Haan, J.F. and Kokke, J.M.M., 1996. Remote sensing algorithm development Toolkit: 1. Operationalization of atmospheric correction methods for tidal and inland waters. BCRS Report, 91 pp.

Dogliotti, A., Ruddick, K., Nechad, B., Doxaran, D., Knaeps, E.,"A single algorithm to retrieve turbidity from remotely-sensed data in all coastal and estuarine waters", Remote Sens. Environ., vol. 156, pages 157–168, 2015.

Doxaran, D., Froidefond, J. M., Lavender, S. and Castaing, P. , "Spectral signature of highlyturbid water application with SPOT data to quantify suspended particulatematter concentration", Remote Sensing Environment, Vol. 81, no. 1, pages 149-161, 2002

Doxaran, D., Froidefond, J.-M. and Castaing, P., "Remote-sensing reflectance of turbid sediment dominated waters. Reduction of sediment type variations and changing illumination conditions effects by use of reflectance ratios", Applied Optics, Vol. 42, pages 2623-2634, 2003.

Doxaran, D., Froidefond, J.M., Castaing, P., "A reflectance band ratio used to estimate suspended matter concentrations in sediment-dominated coastal waters", Int. J. Remote Sens., Vol. 23, pages 5079–5085, 2010.

Frouin R. and B. Pelletier Bayesian methodology for inverting satellite ocean-color data Remote Sensing of Environment, 159 (2015), pp. 332–360.

Guanter, L., Ruiz-Verdu, A., Odermat, D., Giardino, C., Simis, S., Estelles, V., Heege, T., Dominguez-Gomez, J.-A., Moreno, J., 2010: Atmospheric correction of ENVISAT/MERIS data over inland waters: Validation for European lakes. - Remote Sensing of Environment, 114, 3, pp. 467—480.

Neukermans, G., Ruddick, K.G. and N. Greenwood Diurnal variability of turbidity and light attenuation in the southern North Sea from the SEVIRI geostationary sensor Remote Sensing of Environment, 124 (2012), pp. 564–580

Qiu, Z., "A simple optical model to estimate suspended particulate matter in Yellow River Estuary", Opt. Express, Vol 21, pages 27891–27904, 2013.

Ramon, D., Santer, R., 2005. Aerosol over land with MERIS, present and future. In ESA/ESRIN (Ed.), Proceedings of the MERIS-(A)ATSR workshop. Frascati, Italy

Ruddick, K., G. Lacroix, Y. Park, V. Rousseau, V. De Cauwer, and S. Sterckx, 2008. Overview of Ocean Colour: theoretical background, sensors and applicability for the detection and monitoring of harmful algae blooms (capabilities and limitations). Real-time coastal observing systems for ecosystem dynamics and harmful algal blooms. M. Babin, C.S. Roesler and J.J. Cullen, eds. UNESCO Publishing, Paris, France p 331 – 384.

Rymszewicz, A., O'Sullivan, J.J., Bruen, M., Turner, J., Lawler, D., Conroy, E., Kelly-Quinn, M. Implications of Variability of Optical Turbidity Measurements for Different Sensors in Water Quality Monitoring Programmes (http://epa.smartsimple.ie/files/347278/105778/Turbidity_first_paper_full_forreview.docx)

Sterckx, S., Knaeps, E. and Ruddick, K.. (2011). Detection and Correction of Adjacency Effects in hyperspectral airborne data of Coastal and Inland Waters: the Use of the Near Infrared Similarity Spectrum, International Journal of Remote Sensing,Vol. 32:21, 6479-6505.

Tassan, S., "Local algorithms using SeaWiFS data for the retrieval of phytoplankton, pigments, suspended sediment, and yellow substance in coastal waters" Appl. Opt., Vol 33, pages 2369–2378, 1994.

Verhoef, W. and Bach, H. 2003. Simulation of hyperspectral and directional radiance images using coupled biophysical and atmospheric radiative transfer models. Remote Sensing of Environment, 87: 23–41